Supporting Information

Isolation of the elusive $[Ru(bipy)_3]^+$: a key intermediate in photoredox catalysis.

Samuel J. Horsewill,[a] Chengyang Cao,[b] Noah Dabney,[c] Eric S. Yang,[b] Stephen Faulkner[b] and Daniel J. Scott*[a]

[a] Department of Chemistry, University of Bath, Claverton Down, Bath, BA2 7AY, United Kingdom

[b] Department of Chemistry, Chemistry Research Laboratory, University of Oxford, 12 Mansfield Road, Oxford, OX1 3TA, United Kingdom

[c] Department of Chemistry, Guilford College, 5800 W Friendly Ave., Greensboro, NC 27410 (US)

*E-mail: ds2630@bath.ac.uk

Contents

1 Methods

1.1 General experimental procedures

Unless stated otherwise, all reactions, manipulations and spectroscopic acquisitions were performed under an N_2 or Ar atmosphere (< 0.1 ppm O_2, H_2O) through use of MBraun Labmaster or MBraun MB20G gloveboxes and standard Schlenk line techniques. All glassware was oven dried (>160 °C) overnight prior to use.

Hexane and toluene were collected from an Innovative Technologies inc. PS-400-7 solvent purification system before being degassed and stored over molecular sieves (3 Å). THF was pre-dried over activated molecular sieves (3 Å), then dried in a sodium/benzophenone still, before being degassed and stored over molecular sieves (3 Å). CH_3CN was pre-dried over activated molecular sieves (3 Å), then dried in a calcium hydride still, before being degassed and stored over molecular sieves (3 Å). CD_3CN was dried by refluxing over CaH_2, then was degassed and distilled before being stored over molecular sieves (3 Å). KC_8 was prepared according to literature procedure.[1] Unless otherwise stated, $[Ru(bipy)_3]Cl_2{\cdot}6H_2O$ and all other starting materials were purchased from major suppliers. $[Ru(bipy)_3]Cl_2{\cdot}6H_2O$ was dehydrated by heating to 60 °C with stirring under vacuum overnight. Unless supplied under inert atmosphere or noted otherwise, all other solids were dried under vacuum and liquids were degassed and dried over molecular sieves (3 Å).

NMR spectra were recorded on a Bruker Avance (400 MHz), Bruker Neo (400 MHz), or an Agilent ProPulse (500 MHz) spectrometer. Chemical shifts, *δ*, are reported in parts per million (ppm); ^{1}H and ^{13}C NMR shifts were referenced externally to $SiMe_4$ and referenced internally to residual solvent peaks, while ^{31}P NMR shifts were referenced externally to 85% H_3PO_4 (aq.), and ^{11}B NMR shifts were referenced externally to 15% $BF_3.OEt_2$ in $CDCl_3$. The abbreviations s, d, t, q, m are used to indicate singlets, doublets, triplets, quartets and multiplets respectively. Except where indicated otherwise, integrals for $^{31}P\{^{1}H\}$ and ^{31}P spectra are provided for the purposes of qualitative comparison only and should not be considered quantitatively accurate.

EPR spectra were recorded at room temperature on a Bruker EMXmicro X-band continuous wave EPR spectrometer at the CAESR facility at the University of Oxford. UV-vis spectra were recorded at room temperature using an Ocean Optics assembly with an Ocean Optics DH2000 light source and Ocean Insight Flame miniature spectrometer, using fibre-optic cables to pass light through a sample in the glovebox. Elemental analysis was performed by Orla McCullough at London Metropolitan University, with each measurement performed in duplicate either with a combustible ([**Ru**]Cl_2, [**Ru**][BPh_4]) or without ([**Ru**]Cl) and provided alongside a separately measured standard (acetanilide). We attribute the C and N values being slightly below the calculated values for [**Ru**]Cl_2 and [**Ru**]Cl to incomplete combustion. Mass spectrometry was performed by Paul Gates at the University of Bristol, on samples dissolved in DCM/MeCN (50%) and run in positive mode with nanospray ionisation using an Advion Nanomate chip-based nanospray system attached to a Waters Synapt G2S Mass Spectrometer.

1.2 LED apparatus

The LED apparatus used was the same as that in a recent publication.[2] For clarity, this information is reproduced here. Individual LEDs are mounted to a heatsink plate, with the six-LED array powered by a 28 W power supply. The sample block was kept cool by circulation of cooling water, and JY NMR tubes were positioned above the LEDs in a bath of deionised water to assist with thermal transfer. The LEDs used for this study are listed below:

Luminus SST-10-UV-A130, UV (365 nm)

Osram OSLON SSL 120, Deep Blue (455 nm)

Osram OSLON SSL 120, Green (530 nm)

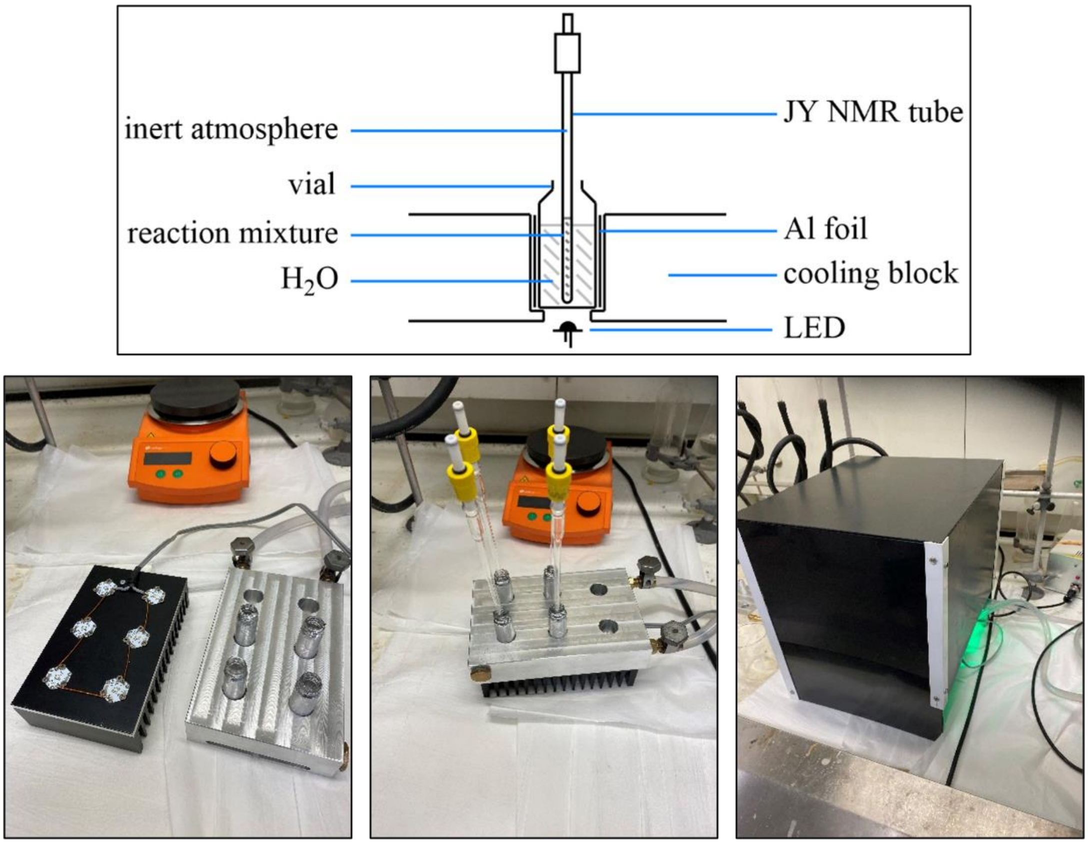

Figure S1: Illustration and photographs of the apparatus used for photochemical experiments. Similar apparatus has been described previously by the Wolf group.[3] Illustration not to scale. Sockets in cooling block have diameter 1.8 cm to fit vials. Base of vial is* ca. *9 mm above the LEDs.

2 Synthesis and characterisation

2.1 Preparation of [Ru]Cl_2

A Schlenk flask was charged with [Ru(bipy)$_3$]Cl_2·6H_2O (*ca.* 5 g) and heated to 60 °C with stirring *in vacuo* for 16 h. A colour change from red to orange was observed as the water was driven off. An NMR spectrum was recorded in CD_3CN, showing complete dehydration.

^{1}H NMR (CD_3CN): δ = 8.65 (dt, J = 8.3, 1.1 Hz, 6H, **bipy**), 8.06 (ddd, J = 8.2, 7.6, 1.5 Hz, 6H, **bipy**), 7.73 (ddd, J = 5.6, 1.5, 0.7 Hz, 6H, **bipy**), 7.40 (ddd, J = 7.7, 5.6, 1.3 Hz, 6H, **bipy**).

UV-vis (CH_3CN): λ_{max} (ε) = 245 (2.92 x10^4), 289 (3.83 x10^4), 447 nm (1.87 x10^4 M^{-1} cm^{-1}).

Elemental Analysis: Anal. Calcd. for [**Ru**]Cl_2: C, 56.25%; H, 3.78%; N, 13.12%. Found: C, 55.46-55.90%; H, 3.77-3.93%; N, 12.79-12.86%.

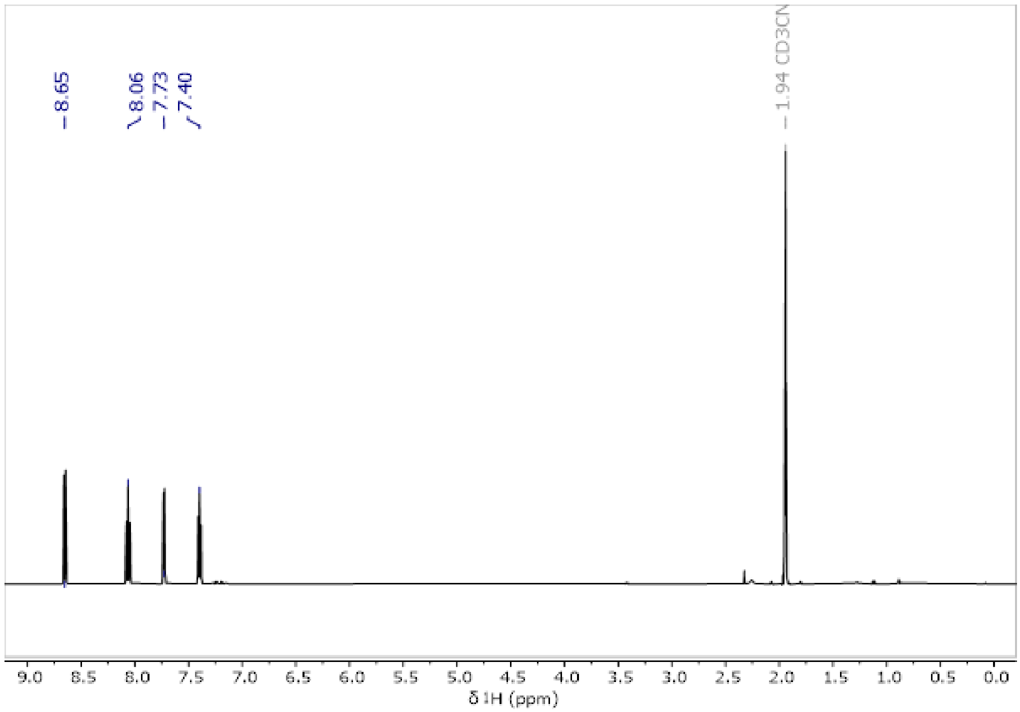

***Figure S2:** ^{1}H NMR spectrum of [Ru]Cl_2 recorded in CD_3CN. Assignment: bipy, δ = 8.65, 8.06, 7.73 and 7.40 ppm.*

2.2 Synthesis and characterisation of [Ru]Cl

A Schlenk flask was charged with [**Ru**]Cl_2 (200.2 mg, 0.313 mmol) and KC_8 (51.4 mg, 0.380 mmol), then THF (30 mL) was added with stirring. An immediate colour change from orange to pink-red was observed and the mixture was stirred for a further 1 hr. After setting up a Soxhlet extraction apparatus and flushing it with nitrogen, the suspension was transferred *via* cannula into the extraction cup *in situ*. Soxhlet extraction was then performed, using a total of 60 mL THF and refluxing for 20 hr. The solids were occasionally agitated inside the extraction cup using a magnetic stirrer bar and a magnet outside the vessel. THF was removed from the filtrates under vacuum, leaving [**Ru**]Cl as a dark red solid, which was washed with hexane (3x 10 mL), then dried and weighed (50.0 mg, 0.0781 mmol, 25%). As expected, no resonances were observed in the ^{1}H NMR spectrum of this material.

UV-vis (CH_3CN): λ_{max} (ε) = 244 (1.48 x10^4), 290 (3.04 x10^4), 341 (0.89 x10^4), 491 nm (0.75 x10^4 M^{-1} cm^{-1}).

Elemental analysis: Anal. Calcd. for [**Ru**]Cl: C, 59.55%; H, 4.00%; N, 13.89%. Found: C, 57.72-57.73%; H, 4.18-4.19%; N, 12.11-12.36%.

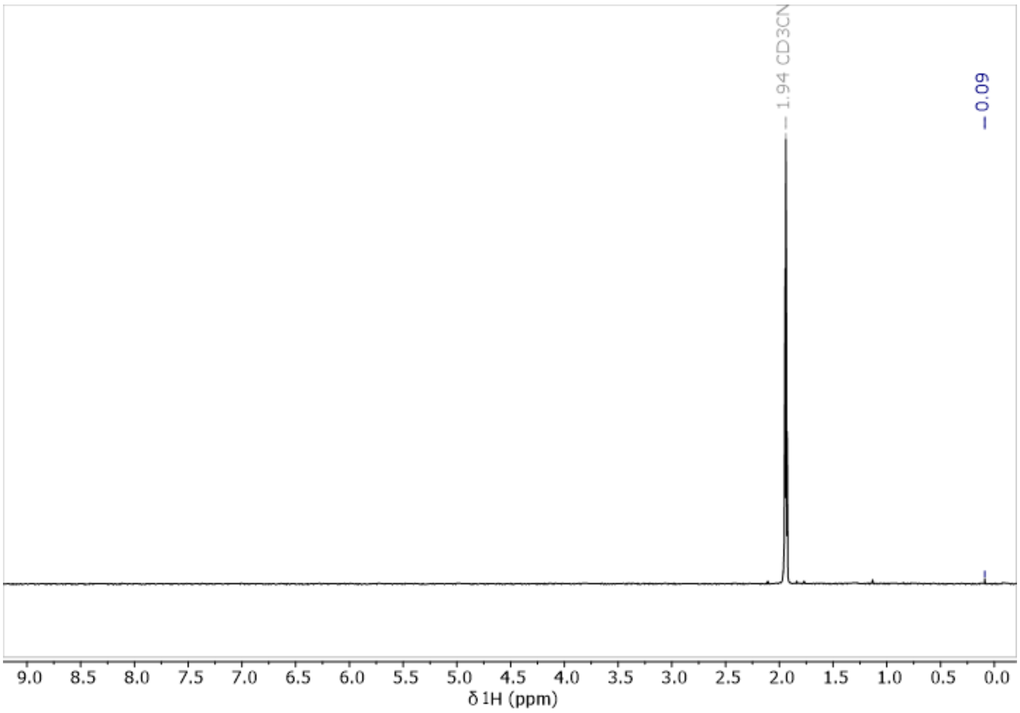

Figure S3: ***[1]H NMR spectrum of [Ru]Cl recorded in CD_3CN. The resonance at 0.09 ppm is assigned to a small quantity of silicone grease resulting from the Soxhlet extraction.***

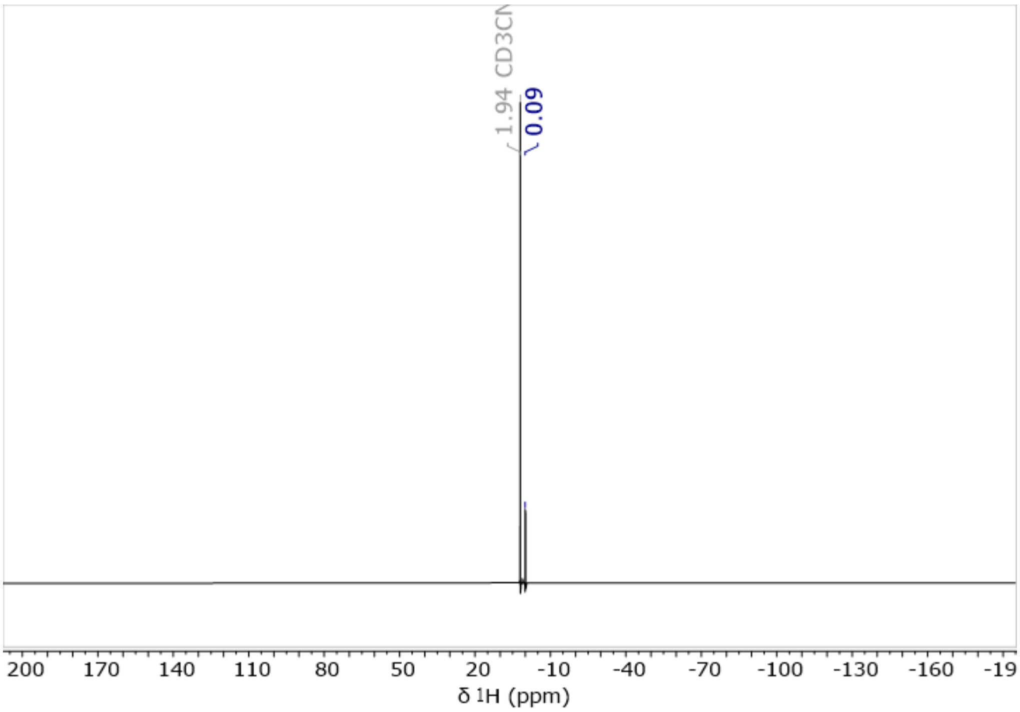

Figure S4: ***[1]H NMR spectrum of [Ru]Cl recorded in CD_3CN using a 400 ppm sweep width.***

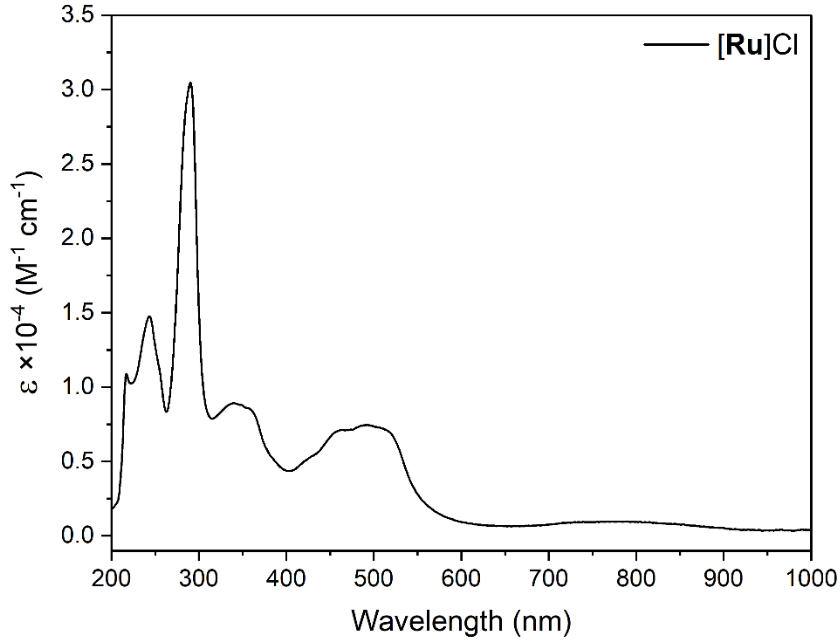

Figure S5: UV-vis absorption spectrum of [Ru]Cl, recorded on a 500 µM solution in MeCN using a 1 mm path length cuvette.

2.3 Synthesis and characterisation of [Ru][BPh_4]

A Schlenk flask was charged with [**Ru**]Cl_2 (931 mg, 1.45 mmol) and KC_8 (223 mg, 1.64 mmol), then THF (50 mL) was added with stirring. An immediate colour change from orange to pink-red was observed and the mixture was stirred for a further 2 hr. The suspension was transferred onto Na(BPh_4) (497 mg, 1.45 mmol) and stirred for a further 1.5 hr. THF was removed *in vacuo* and the resulting dark red solids were transferred to a Soxhlet extraction cup. A Soxhlet extraction was performed, using 75 mL THF and refluxing for 44 hr. THF was removed from the filtrates, leaving a dark red solid, which was washed thoroughly with hexanes (3x 10 mL). The solids [**Ru**][BPh_4] were then dried and weighed (697 mg, 0.784 mmol, 54% yield). Recrystallisation from a saturated MeCN solution at -35 °C provided analytically pure [**Ru**][BPh_4]. The 1:1 ratio of Ru to the BPh_4 anion in [**Ru**][BPh_4] was confirmed by NMR integration relative to a known quantity of [NEt_4][PF_6] as an internal standard.

^{1}H NMR (CD_3CN): δ = 6.80 (t, 7.2 Hz, 4H, **BPh₄**), 6.96 (t, 7.4 Hz, 8H, **BPh₄**), 7.2 ppm (t, br, 8H, **BPh₄**).

^{13}C NMR (CD_3CN): δ = 135.9 (**BPh₄**), 125.8 (**BPh₄**), 122.1 ppm (**BPh₄**).

^{11}B NMR (CD_3CN): δ = -5.8 ppm (s, **BPh₄**).

UV-vis (CH_3CN): λ_{max} (ε) = 240 (3.23 x10^4), 292 (3.95 x10^4), 342 (1.84 x10^4), 497 nm (1.36 x10^4 M^{-1} cm^{-1}).

Elemental analysis: Calcd. for [**Ru**][BPh_4].MeCN: C, 72.33%; H, 5.09%; N, 10.54%. Found: C, 72.11-72.55%; H, 4.78-5.05%; N, 10.65-10.73%.

Mass Spectrometry: Predicted for [**Ru**]$^+$ (C30 H24 N6 Ru), *m/z* = 570.1106; Found, *m/z* = 570.1167.

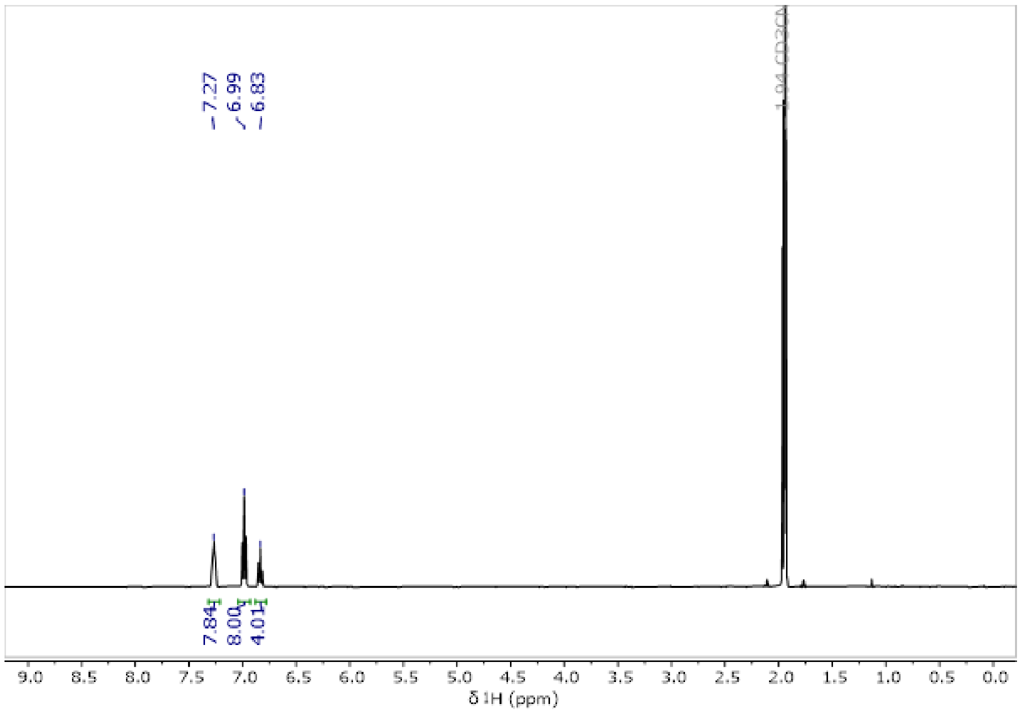

***Figure S6:** ^{1}H NMR spectrum of [Ru][BPh_4] recorded in CD_3CN. Assignment: [BPh_4]$^-$, δ = 7.27, 6.99 and 6.83 ppm.*

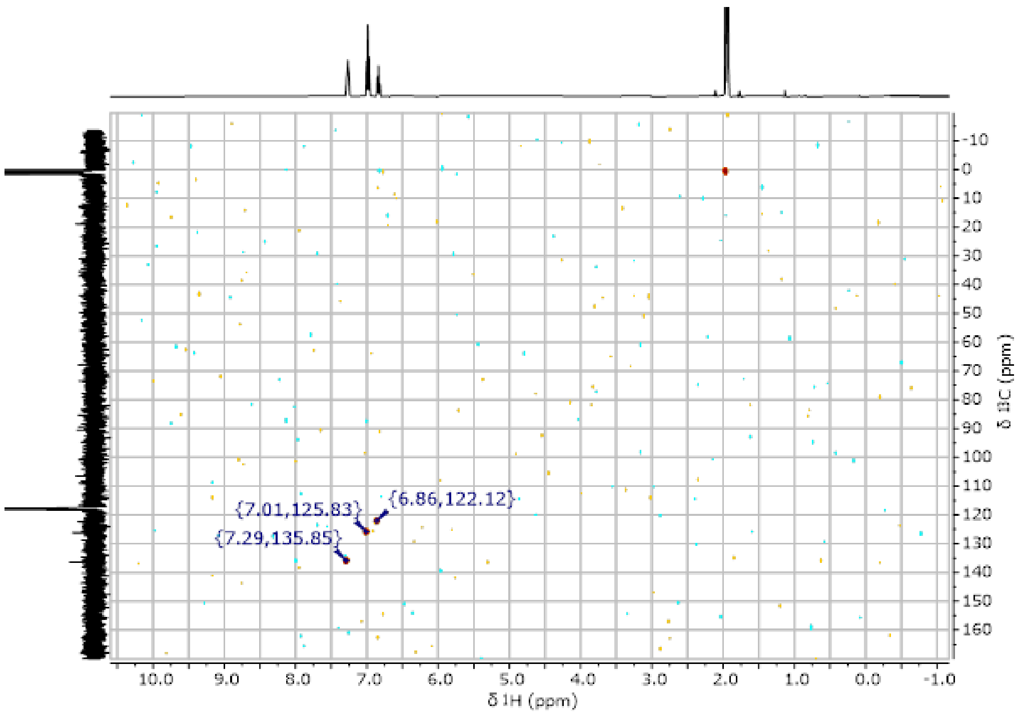

Figure S7: $^{1}H/^{13}C$ HSQC NMR spectrum of [Ru][BPh_4] recorded in CD_3CN. Assignment (^{13}C): [BPh_4]$^-$, δ = 135.9, 125.8 and 122.1 ppm; CD_3CN, δ = 117.8 and 0.9 ppm.

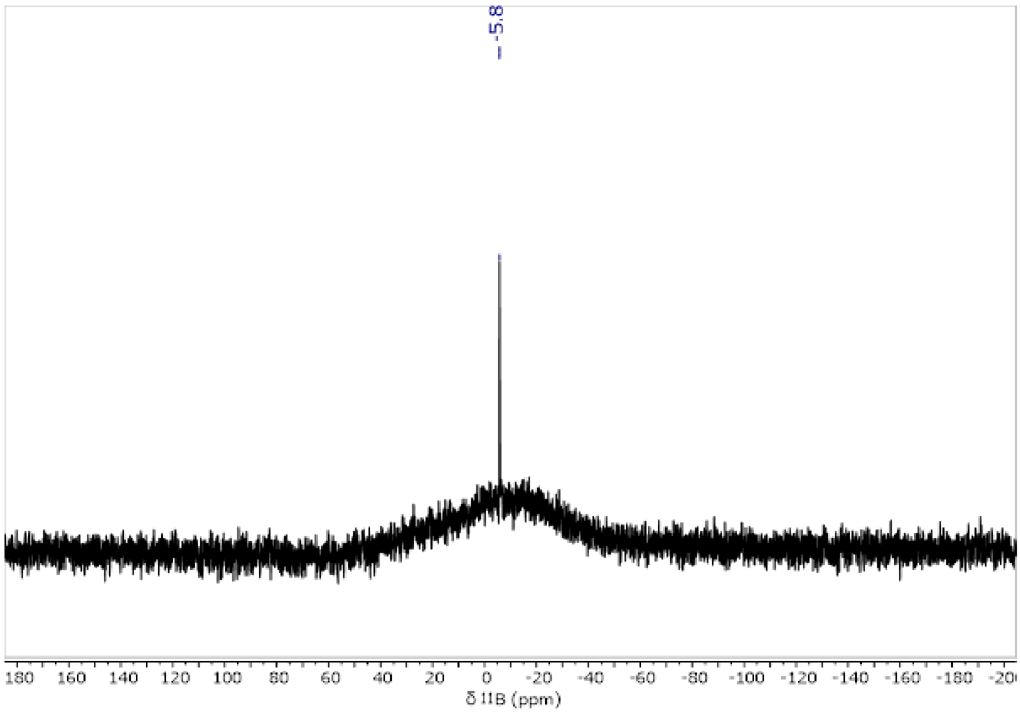

Figure S8: $^{11}B\{^{1}H\}$ NMR spectrum of [Ru][BPh_4] recorded in CD_3CN. Assignment: [BPh_4]$^-$, δ = 5.8 ppm.

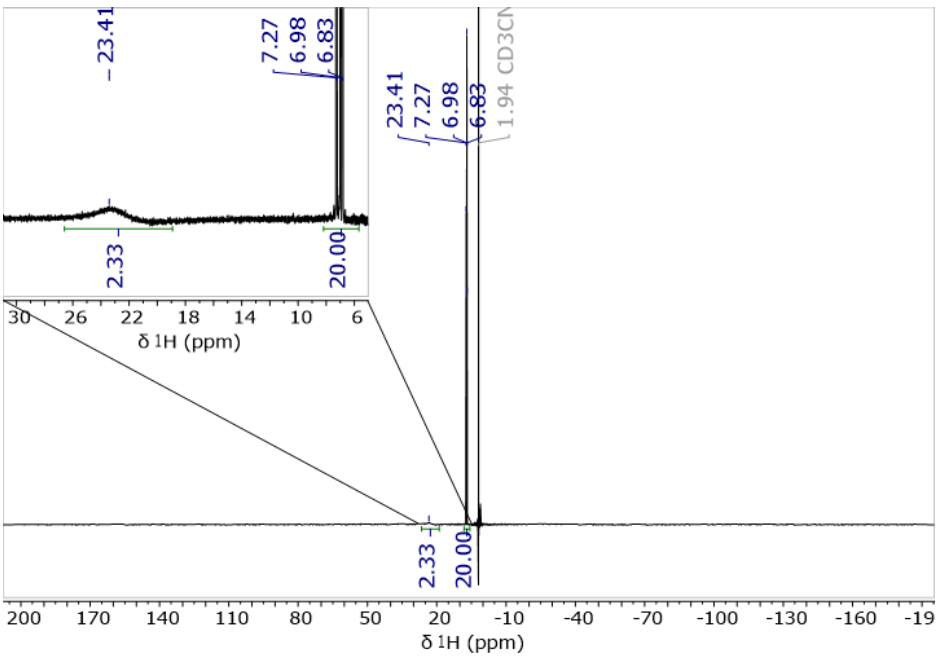

Figure S9: ¹H NMR spectrum of [Ru][BPh₄], recorded in CD₃CN using a 400 ppm sweep width. Assignment: [BPh₄]⁻, δ = 7.27, 6.98 and 6.83 ppm; (bipy)⁻, δ = 23.41 ppm. Inset is an expansion showing the resonance at δ = 23.41 ppm more clearly.

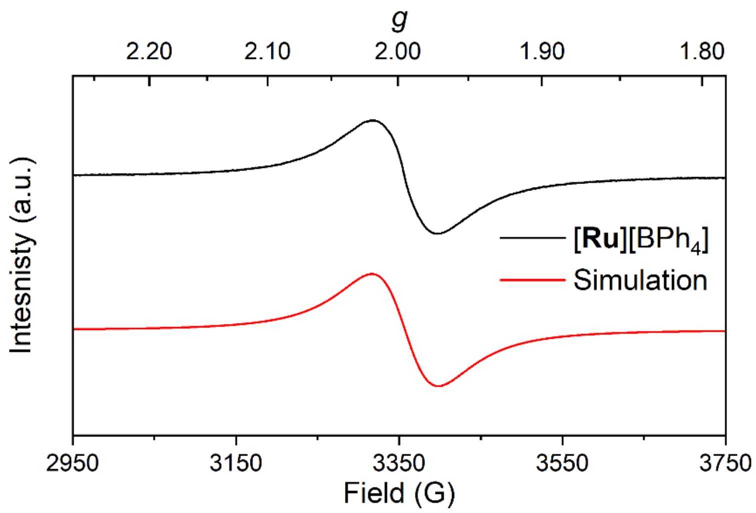

Figure S10: X-band EPR spectrum of [Ru][BPh₄], recorded on a 2 mM MeCN solution at room temperature. Microwave frequency 9.3722 GHz, power 20 mW, simulated with g = 2.002.

3 Reactivity

All the following reactions were performed in NMR tubes, using the same volume and using identical concentrations of substrates and photocatalysts, unless noted otherwise. The chosen concentration of [**Ru**][BPh_4] and [**Ru**]Cl_2 used was 2.5 mM, and substrates (PhCl, PhBr and PhI) and radical traps ($P(OMe)_3$, B_2pin_2) were used at 50 mM concentrations. All reactions were performed in acetonitrile, and where appropriate 1 eq. of an internal standard (Ph_3PO) was added for the purposes of quantifying the products formed.

We note that ethylamine can be identified in many of our ^1H NMR spectra (δ = 2.32, 1.17 ppm). This was present in the H_3-acetonitrile solvent as purchased from several suppliers, and is a common impurity typically present when MeCN is used as a solvent. We do not believe it is relevant to the observed reactivity as its concentration was significantly lower (*ca.* 20 times lower) than the substrates used, and this concentration did not appear to change over the course of the experiments.

Quantification of [**Ru**]$^{2+}$ reformed during a reaction was achieved by ^1H NMR integration against the [BPh_4]$^-$ resonances. Quantification in ^{31}P NMR spectra was achieved using an inverse-gated proton decoupled experiment. We recently confirmed the accuracy of this method for our system by integration of solutions containing known, similar concentrations of the predicted product and the internal standard.[2]

3.1 Photostability studies

We found [**Ru**]Cl and [**Ru**][BPh_4] to be stable in dry, oxygen-free solvents for at least a week at room temperature. To determine the photostability of [**Ru**][BPh_4], solutions of [**Ru**][BPh_4] were irradiated using light of 365, 455 or 530 nm for 16 h (see Figure S11 to Figure S13). Under irradiation at 365 and 455 nm, resonances consistent with the oxidised $[Ru(bipy)_3]^{2+}$ were observed in moderate quantities. However, under irradiation at 530 nm, only a very small quantity of $[Ru(bipy)_3]^{2+}$ was observed (*ca.* 4%). The UV-vis absorption spectra of these reactions show the same trend, with 530 nm light resulting in very minor changes compared to [**Ru**][BPh_4] (Figure S14). Over a 1 h experiment, no $[Ru(bipy)_3]^{2+}$ was detected by ^1H NMR following irradiation by 530 nm light (see Figure S15). In order to establish whether [**Ru**][BPh_4] reacted with the radical trap $P(OMe)_3$ in isolation, a solution containing [**Ru**][BPh_4] and $P(OMe)_3$ was irradiated at 530 nm for 1 h (see Figure S16 and Figure S17). No species other than starting materials were observed in the ^1H or $^{31}P\{^1H\}$ NMR spectra after this time. Likewise, the UV-vis spectrum of this solution showed no significant changes from [**Ru**][BPh_4] (Figure S18).

We also investigated the photostability of [**Ru**]Cl_2 under our experimental conditions by irradiating solutions of [**Ru**]Cl_2 using light of either 455 or 530 nm (see Figure S19 and Figure S20). It was clear from these experiments that significant decomposition had occurred in both cases, but that significantly greater degradation occurred under irradiation by 455 nm than 530 nm light. Solutions of [**Ru**]Cl_2 with radical traps $P(OMe)_3$ and B_2pin_2 were also studied under irradiation (see Figure S21 and Figure S22). With both $P(OMe)_3$ and B_2pin_2, [**Ru**]Cl_2 was consumed and several new resonances were observed to grow in in the aromatic region, similarly to the degradation observed in absence of the radical traps. However, in the case of $P(OMe)_3$ several new resonances were also observed which appeared to arise from reaction between [**Ru**]Cl_2 and $P(OMe)_3$. We presume this to be due to a reduction of [**Ru**]Cl_2. In light of this, we chose to avoid $P(OMe)_3$ and use B_2pin_2 as a radical trap for reactions of [**Ru**]Cl_2.

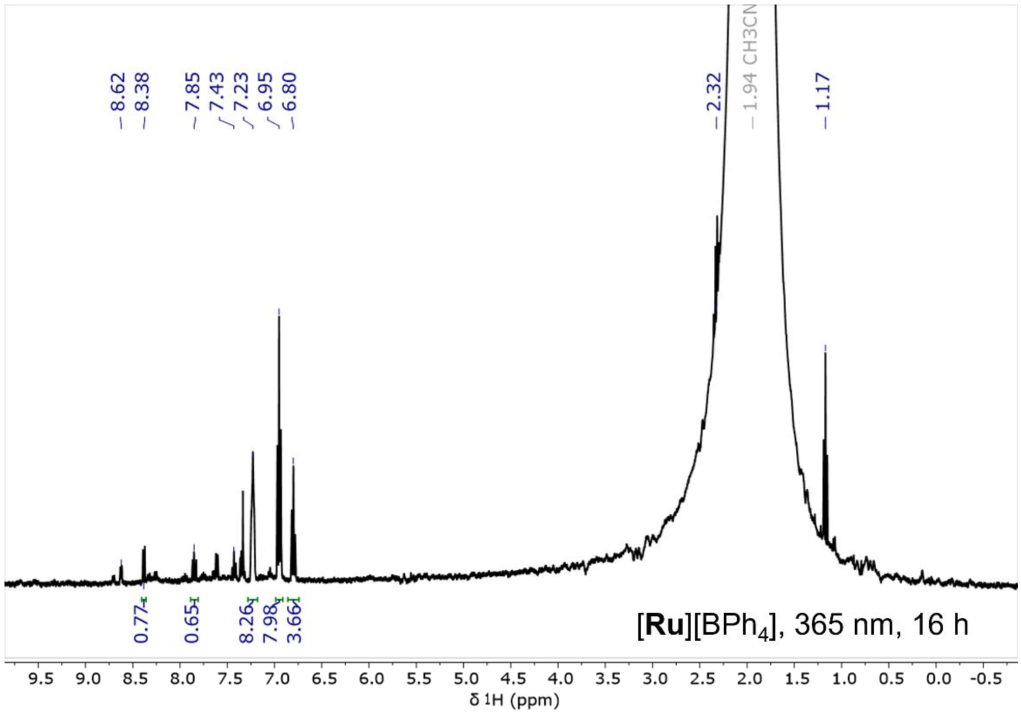

Figure S11: ^{1}H NMR spectrum of [Ru][BPh$_4$] following irradiation by 365 nm light for 16 h. Assignments: [BPh$_4$]$^-$, δ = 7.23, 6.95 and 6.80 ppm; [Ru(bipy)$_3$]$^{2+}$, δ = 8.62, 8.38, 7.85 and 7.43 ppm.

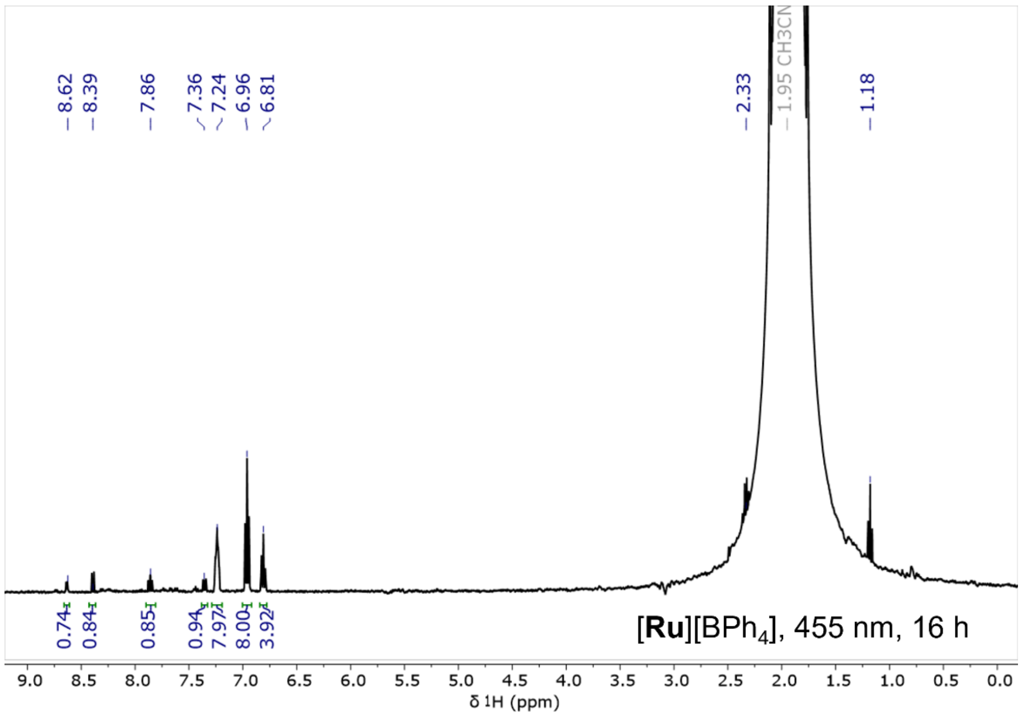

Figure S12: ^{1}H NMR spectrum of [Ru][BPh$_4$] following irradiation by 455 nm light for 16 h. Assignments: [BPh$_4$]$^-$, δ = 7.24, 6.96 and 6.81 ppm; [Ru(bipy)$_3$]$^{2+}$, δ = 8.62, 8.39, 7.86 and 7.36 ppm.

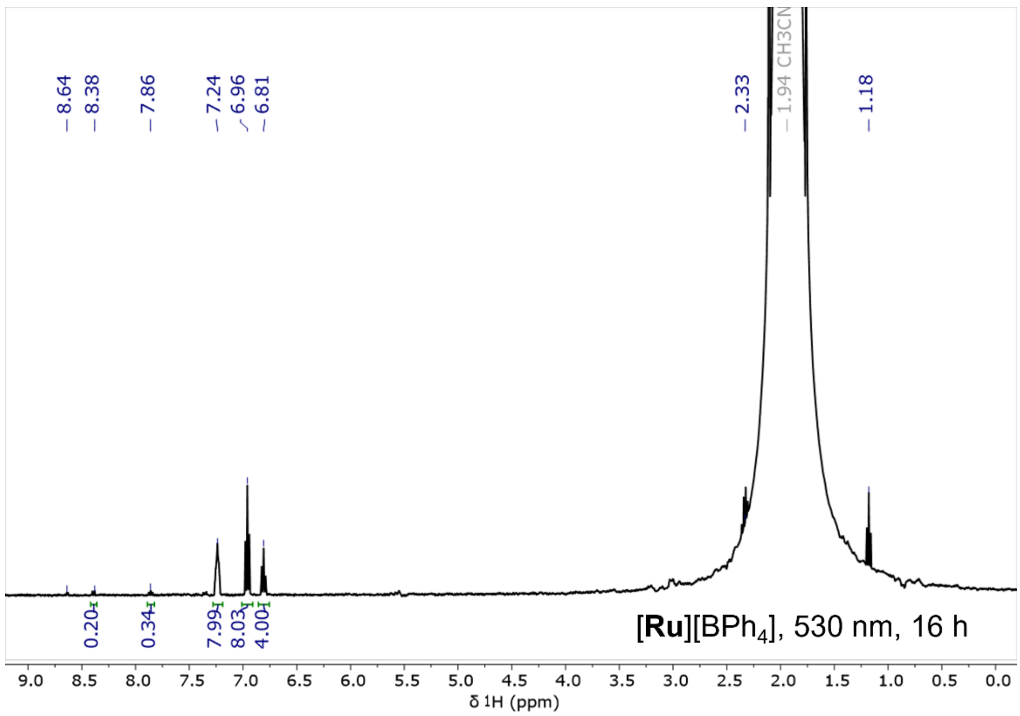

***Figure S13:** *^{1}H NMR spectrum of [Ru][BPh$_4$] following irradiation by 530 nm light for 16 h. Assignments: [BPh$_4$]$^-$, δ = 7.24, 6.96 and 6.81 ppm; [Ru(bipy)$_3$]$^{2+}$, δ = 8.64, 8.38 and 7.86 ppm.**

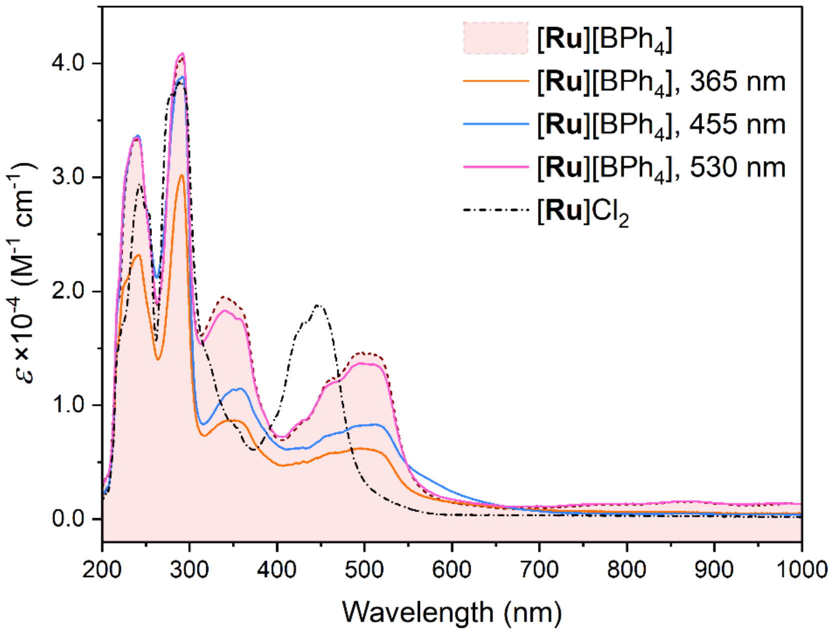

***Figure S14:** *UV-vis absorption spectra of [Ru][BPh$_4$], before and following irradiation by light of 365, 455 or 530 nm for 16 h. Irradiation was performed at 2.5 mM concentration. The solution was then diluted to 500 µM concentration for the UV-vis measurement. Also included is the absorption spectrum of [Ru]Cl$_2$ for comparison.**

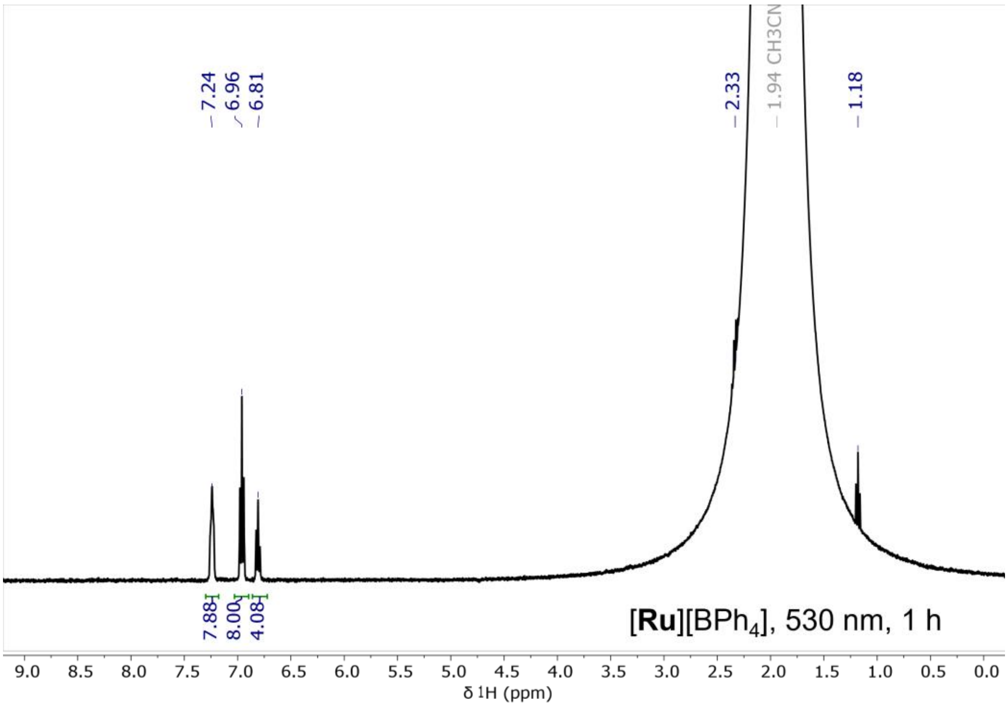

***Figure S15:** ^{1}H NMR spectrum of [Ru][BPh$_4$] following irradiation by 530 nm light for 1 h. Assignments: [BPh$_4$]$^-$, δ = 7.24, 6.96 and 6.81 ppm.*

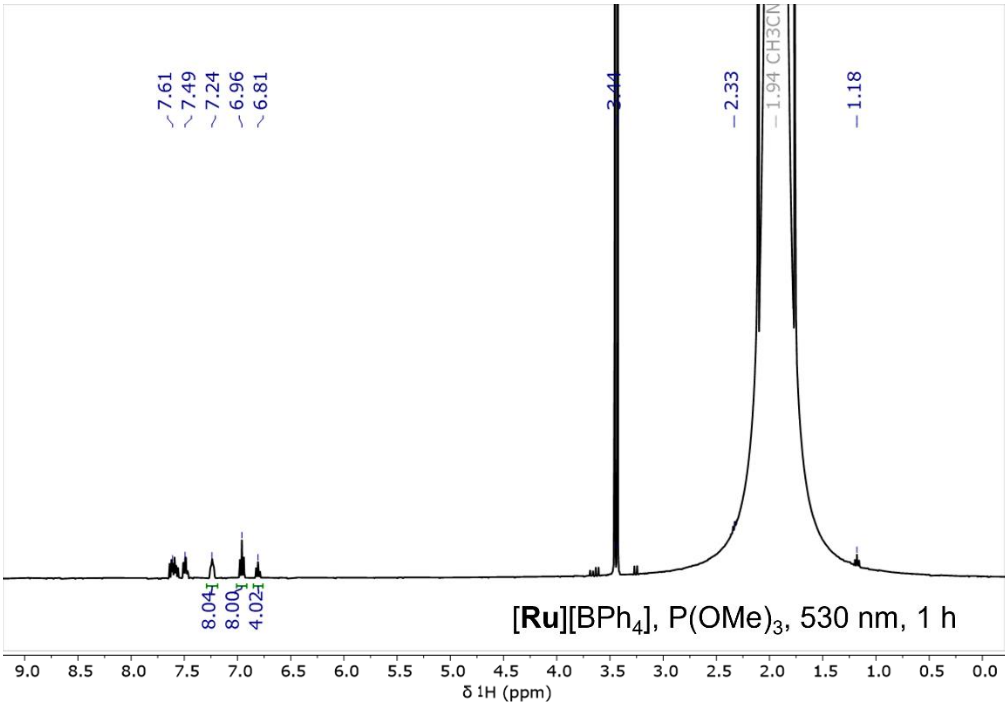

***Figure S16:** ^{1}H NMR spectrum of the reaction between [Ru][BPh$_4$] and P(OMe)$_3$ following irradiation by 530 nm light for 1 h. Ph$_3$PO was added after irradiation. Assignments: [BPh$_4$]$^-$, δ = 7.24, 6.96 and 6.81 ppm; Ph$_3$PO, δ = 7.61-7.49 ppm; P(OMe)$_3$, δ = 3.44 ppm.*

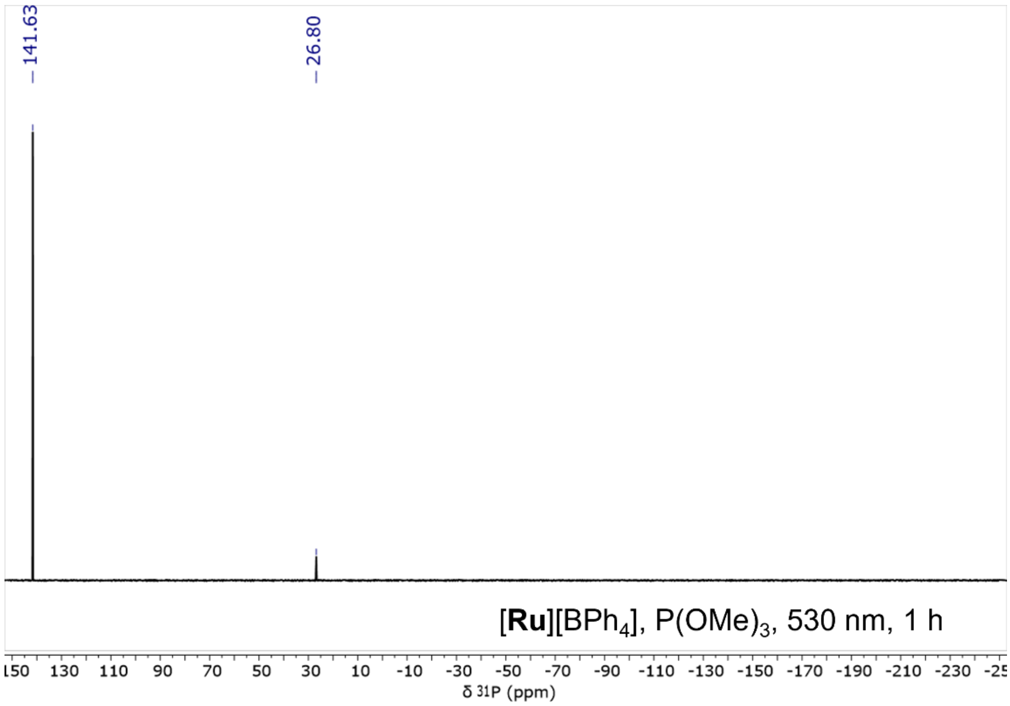

Figure S17: $^{31}P\{^{1}H\}$ NMR spectrum of the reaction between [Ru][BPh$_4$] and P(OMe)$_3$ following irradiation by 530 nm light for 1 h. Ph$_3$PO was added after irradiation. Assignments: P(OMe)$_3$, δ = 141.63 ppm; Ph$_3$PO, δ = 26.80 ppm.

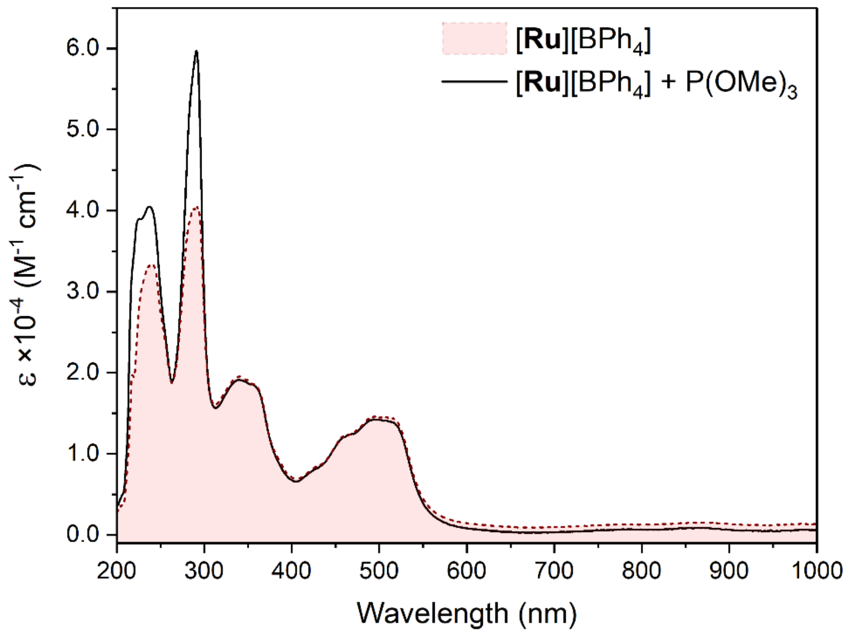

Figure S18: UV-vis absorption spectra of [Ru][BPh$_4$] and P(OMe)$_3$ following irradiation by light of 530 nm for 1 h. The concentration of [Ru][BPh$_4$] was 500 μM, in MeCN. The spectrum of [Ru][BPh$_4$] is included for comparison.

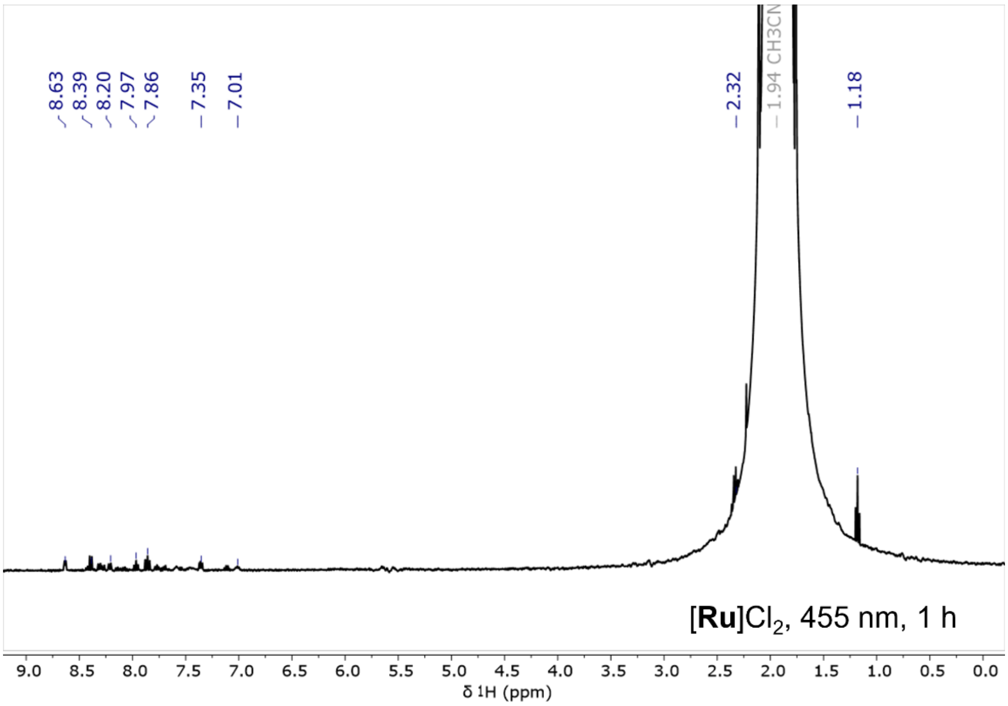

Figure S19: ^{1}H NMR spectrum of [Ru]Cl_2 following irradiation by 455 nm light for 1 h.

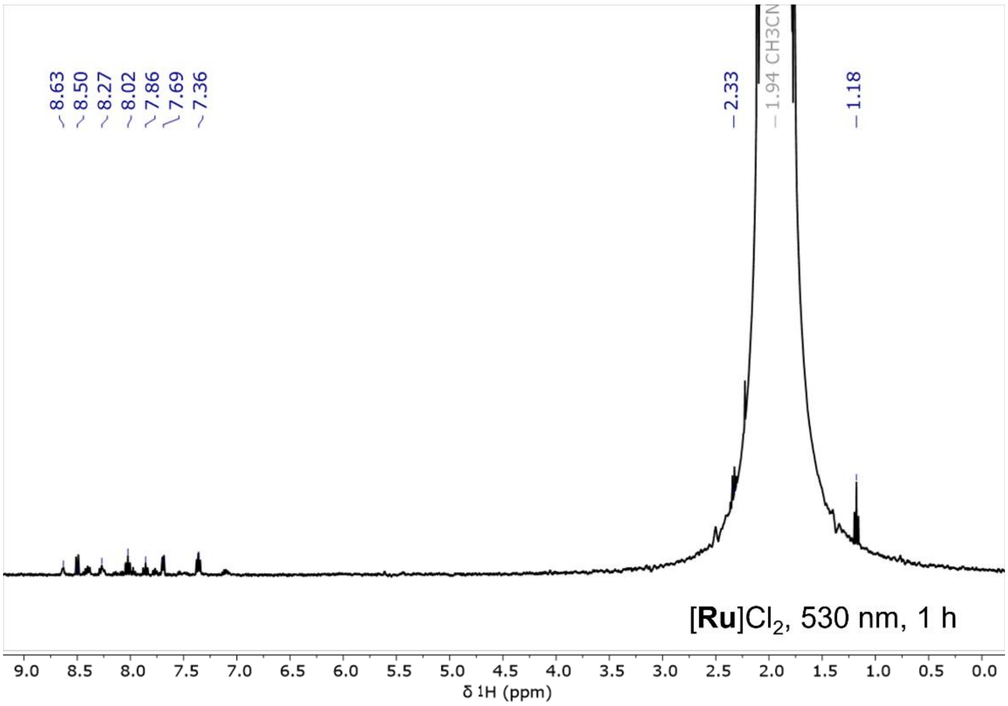

Figure S20: ^{1}H NMR spectrum of [Ru]Cl_2 following irradiation by 530 nm light for 1 h.

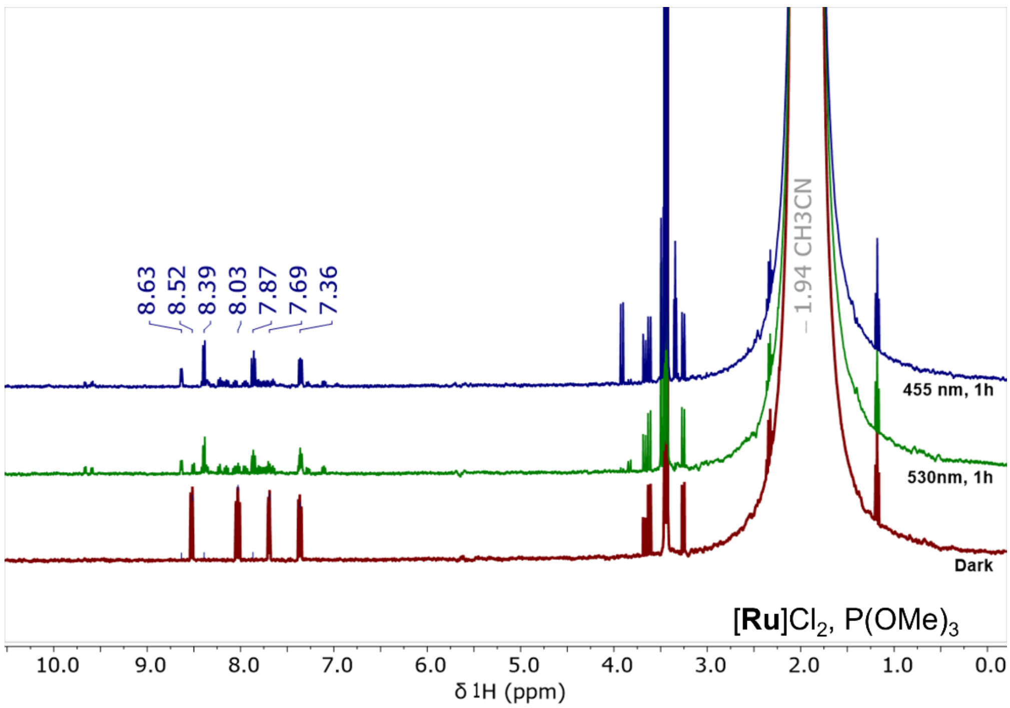

Figure S21: [1]H NMR spectra of the reactions between [Ru]Cl$_2$ and P(OMe)$_3$ in the dark, and following irradiation by 530 or 455 nm light for 1 h. Assignments: [Ru]Cl$_2$, δ = 8.52, 8.03, 7.69 and 7.36 ppm; primary product, δ = 8.63, 8.39, 7.87 and 7.36 ppm.

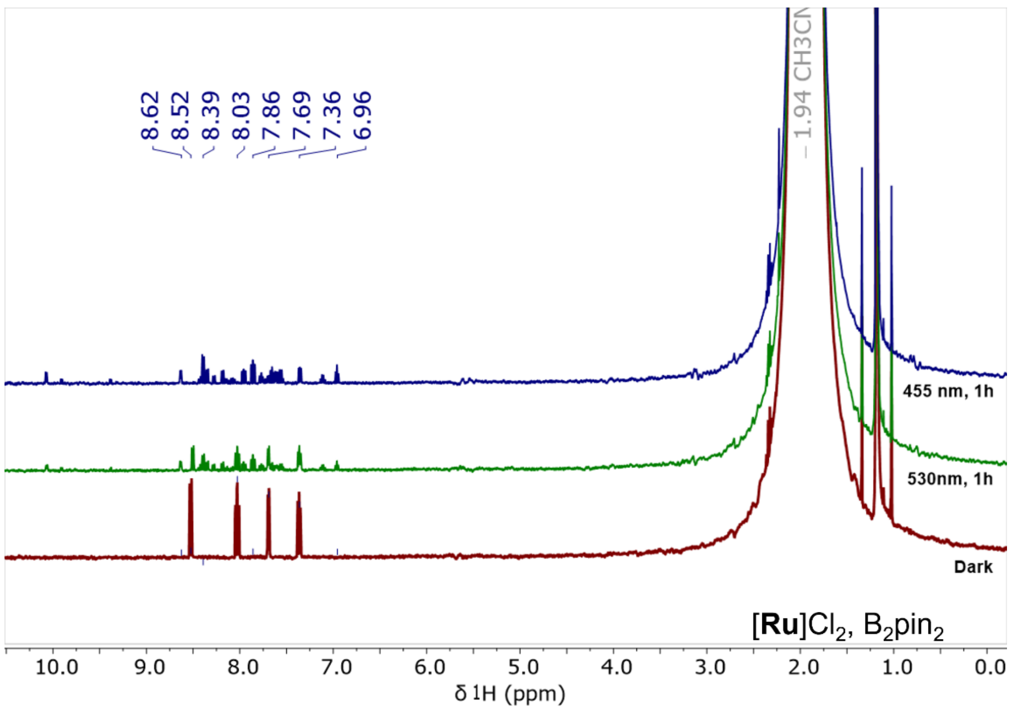

Figure S22: [1]H NMR spectra of the reactions between [Ru]Cl$_2$ and B$_2$pin$_2$ in the dark, and following irradiation by 530 or 455 nm light for 1 h. Assignments: [Ru]Cl$_2$, δ = 8.52, 8.03, 7.69 and 7.36 ppm; primary products, δ = 8.62, 8.39, 7.86 and 6.96 ppm.

3.2 Reduction of aryl halides by [Ru][BPh_4]

To determine any ground-state reactivity, solutions of [**Ru**][BPh_4] with PhCl, PhBr or PhI were left in the dark for 1 h (see Figure S23 to Figure S25). Only the reaction containing PhI resulted in any production of $[Ru(bipy)_3]^{2+}$.

To determine the excited state reactivity, solutions of [**Ru**][BPh_4] with PhCl, PhBr or PhI were irradiated for 1 h with light of 530 nm (see Figure S26 to Figure S28). Reactions containing PhBr and PhI both resulted in resonances consistent with oxidation of [**Ru**][BPh_4] to $[Ru(bipy)_3]^{2+}$.

To confirm that reduction of the aryl halide was responsible for the oxidation of [**Ru**]$^+$ to [**Ru**]$^{2+}$, $P(OMe)_3$ was included to react with the predicted phenyl radicals that would be generated by this reaction. Solutions of [**Ru**][BPh_4] with PhCl, PhBr or PhI and $P(OMe)_3$ were irradiated for 1 h with light of 530 nm (see Figure S29 to Figure S36). In all three cases, the phenyl radical trapping product $PhPO(OMe)_2$ was generated. The highest yield was 60%, for the reaction of [**Ru**][BPh_4] with PhBr. When this reaction was instead run for 16 h, a product yield of 205% was obtained. We presume this high yield to be due to reduction of $[Ru(bipy)_3]^{2+}$ back to $[Ru(bipy)_3]^+$ by $PhP^•(OMe)_3$, the initial product of phenyl radical trapping by $P(OMe)_3$. We recently reported similar observations in photoreactions of organic PCs.[2] Shown in Figures Figure S33 Figure S34 are the ^1H and ^{31}P NMR spectra of $PhPO(OMe)_2$ respectively, where an expansion is shown of the aromatic region of the ^1H NMR spectrum for ease of comparison.

In order to further probe the reactivity, solutions of [**Ru**][BPh_4] were reacted with $MeO(C_6H_4)Cl$ and $MeO_2C(C_6H_4)Cl$ and $P(OMe)_3$ under 530 nm irradiation, also for 1 h (see Figure S37 to Figure S40). Where $MeO(C_6H_4)Cl$ contains an electron donating group making it more challenging to reduce than the parent PhCl, $MeO_2C(C_6H_4)Cl$ contains an electron withdrawing group making it easier to reduce. Accordingly, the yield of the phosphonate product was lower for $MeO(C_6H_4)Cl$ (4%) than for PhCl (12%), while for $MeO_2C(C_6H_4)Cl$ it was higher (17%).

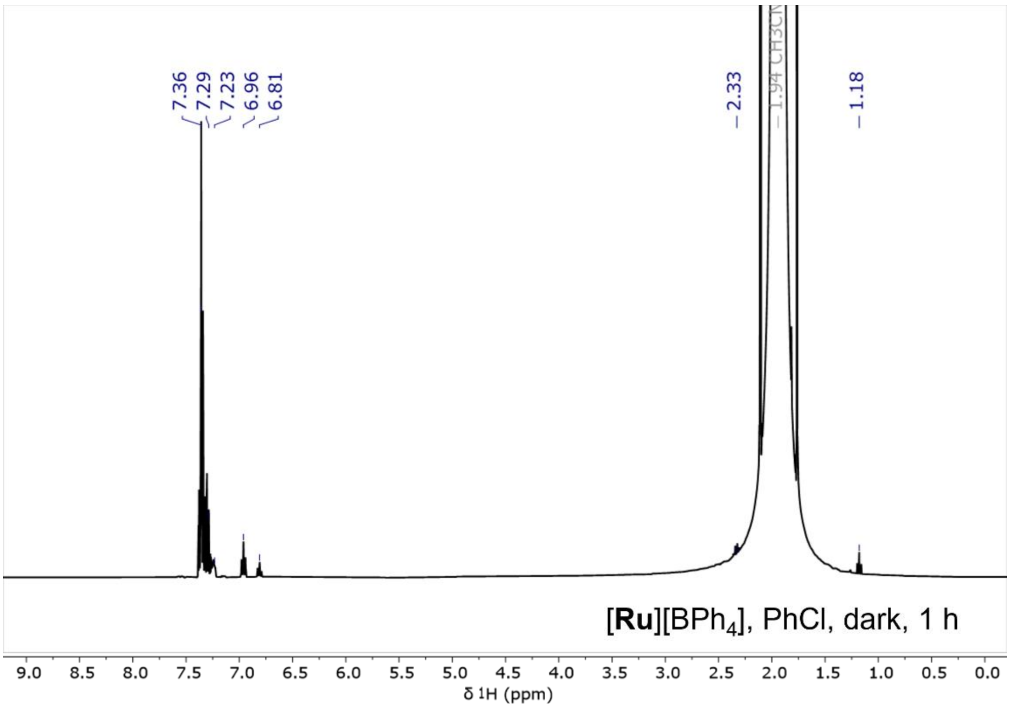

***Figure S23:** ^1H NMR spectrum of the reaction between [Ru][BPh_4] and PhCl after being left in the dark for 1 h. Assignments: $[BPh_4]^-$, δ = 7.23, 6.96 and 6.81 ppm; PhCl, 7.36-7.29 ppm.*

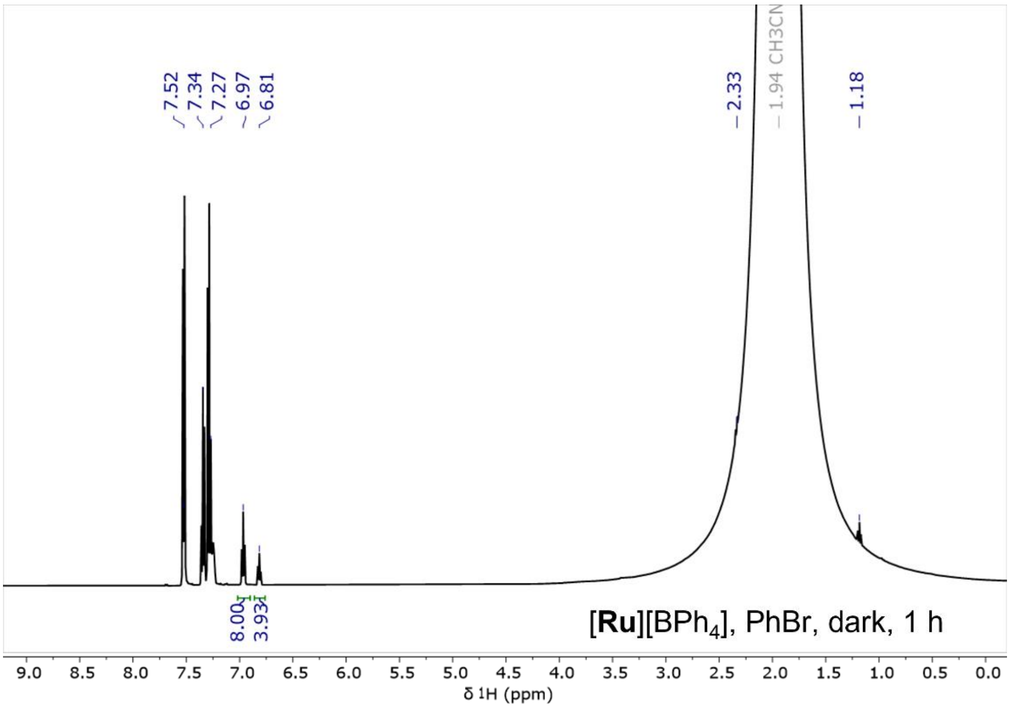

Figure S24: ***^{1}H NMR spectrum of the reaction between [Ru][BPh$_4$] and PhBr after being left in the dark for 1 h. Assignments: [BPh$_4$]$^{-}$, δ = 6.97 and 6.81 ppm; PhBr, 7.52, 7.34-7.27 ppm.***

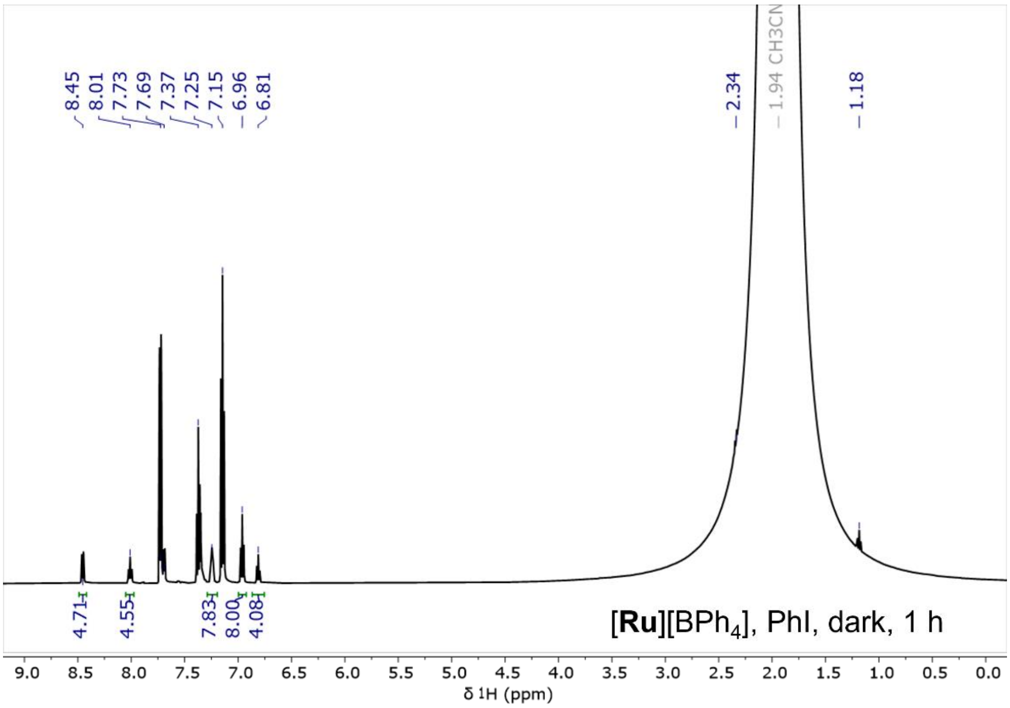

Figure S25: ***^{1}H NMR spectrum of the reaction between [Ru][BPh$_4$] and PhI after being left in the dark for 1 h. Assignments: [BPh$_4$]$^{-}$, δ = 7.25, 6.96 and 6.81 ppm; PhI, δ = 7.73, 7.37 and 7.15 ppm; [Ru(bipy)$_3$]$^{2+}$, δ = 8.45, 8.01 and 7.69 ppm. [Ru(bipy)$_3$]$^{2+}$ recovery: 77%.***

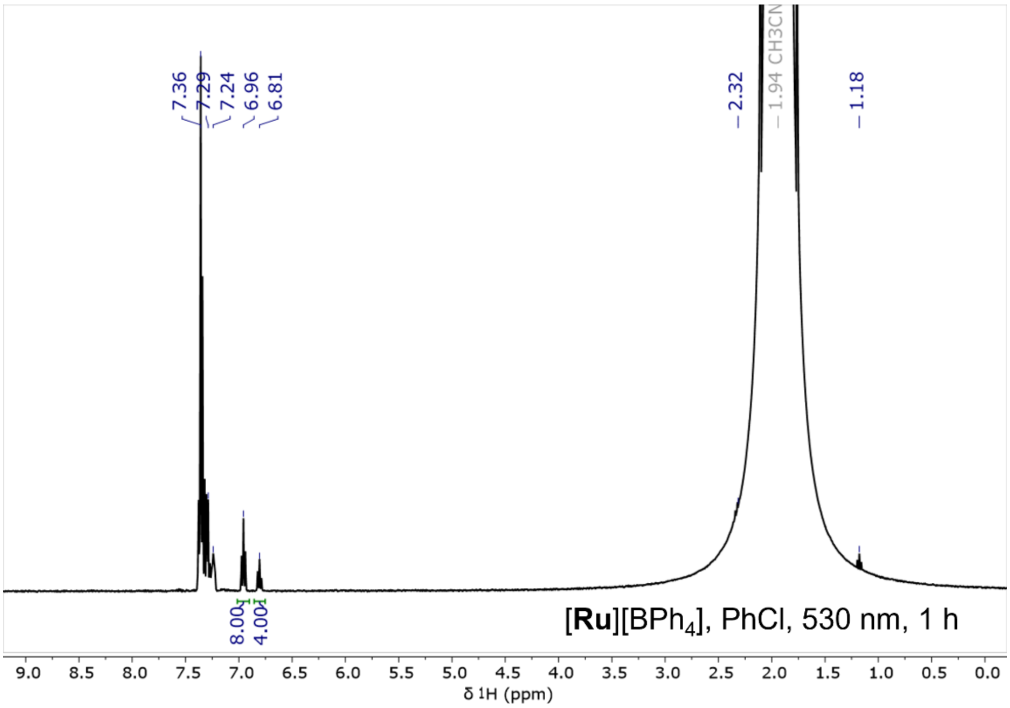

***Figure S26:** ^1H NMR spectrum of the reaction between [Ru][BPh_4] and PhCl following irradiation at 530 nm for 1 h. Assignments: [BPh_4]$^-$, δ = 7.24, 6.96 and 6.81 ppm; PhCl, 7.36-7.29 ppm.*

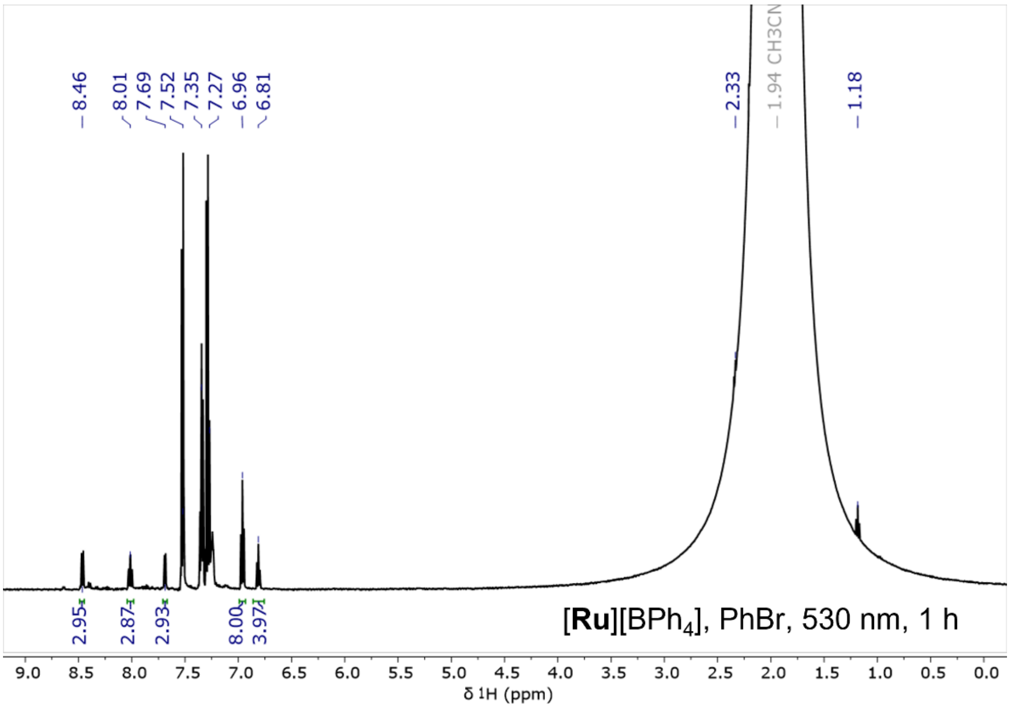

***Figure S27:** ^1H NMR spectrum of the reaction between [Ru][BPh_4] and PhBr following irradiation at 530 nm for 1 h. Assignments: [BPh_4]$^-$, δ = 6.96 and 6.81 ppm; PhBr, δ = 7.52, 7.35-7.27 ppm; [Ru(bipy)$_3$]$^{2+}$, δ = 8.46, 8.01 and 7.69 ppm. [Ru(bipy)$_3$]$^{2+}$ recovery: 49%.*

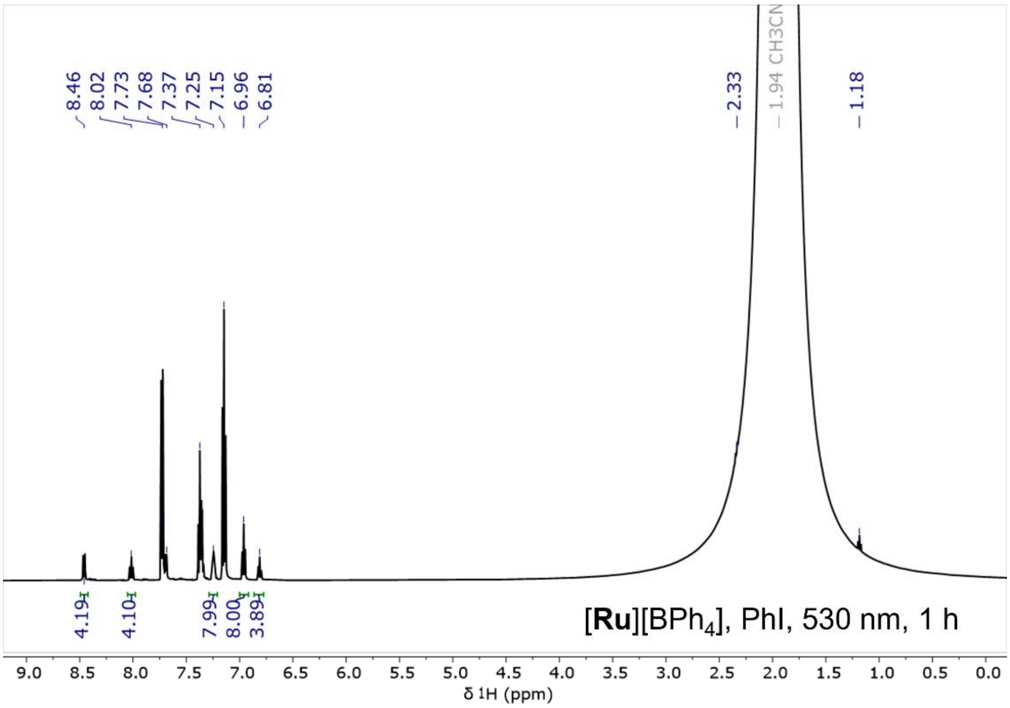

Figure S28: ***^{1}H NMR spectrum of the reaction between [Ru][BPh_4] and PhI following irradiation at 530 nm for 1 h. Assignments: [BPh_4]$^{-}$, δ = 7.25, 6.96 and 6.81 ppm; PhI, δ = 7.73, 7.37 and 7.15 ppm; [Ru(bipy)$_3$]$^{2+}$, 8.46, 8.02 and 7.68 ppm. [Ru(bipy)$_3$]$^{2+}$ recovery: 69%.***

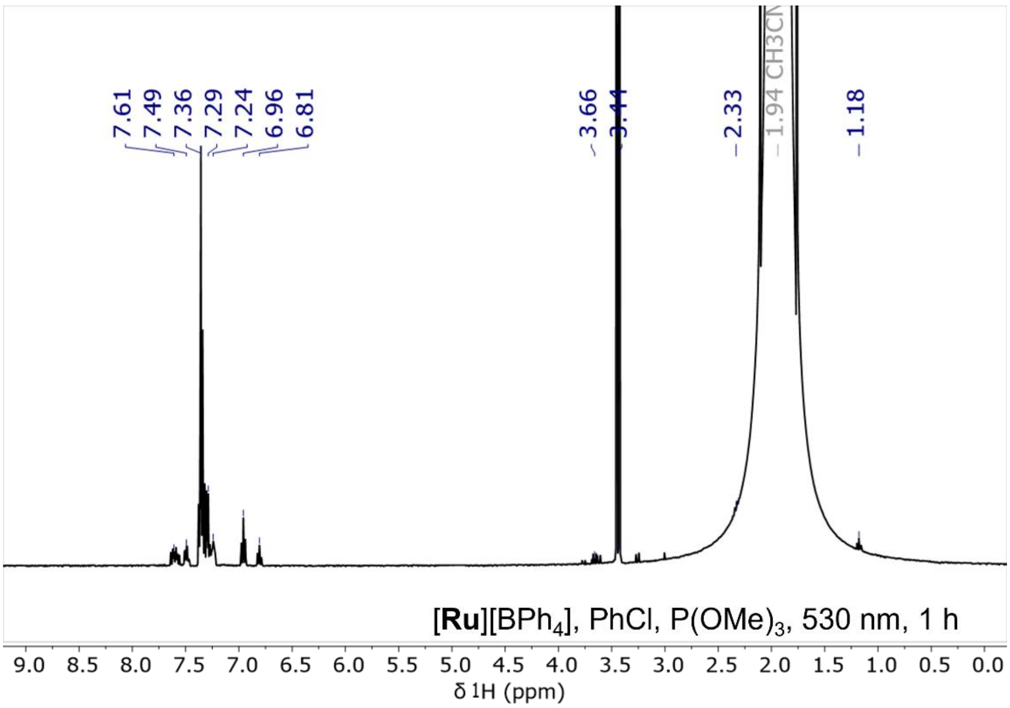

Figure S29: ***^{1}H NMR spectrum of the reaction between [Ru][BPh_4], PhCl and P(OMe)$_3$ following irradiation at 530 nm for 1 h. Assignments: [BPh_4]$^{-}$, δ = 7.24, 6.96 and 6.81 ppm; PhCl, δ = 7.36-7.29 ppm; Ph_3PO, δ = 7.61 and 7.49 ppm; P(OMe)$_3$, δ = 3.44 ppm; PhPO(OMe)$_2$, δ = 3.66 ppm. Ph_3PO was added after the reaction was completed.***

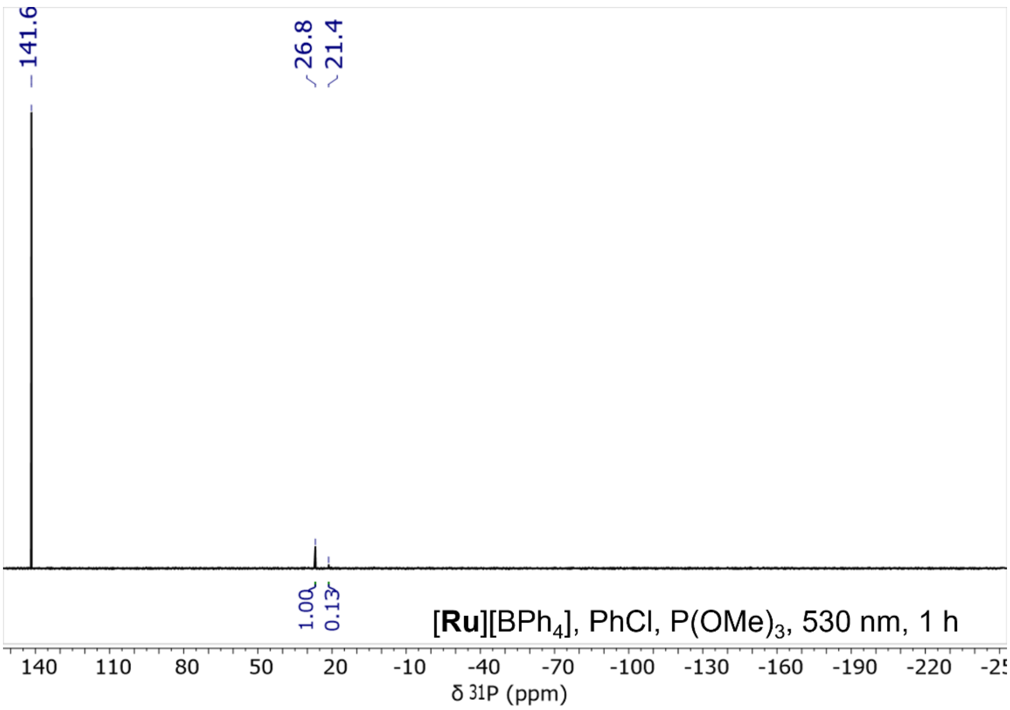

Figure S30: $^{31}P\{^{1}H\}$ NMR spectrum of the reaction between [Ru][BPh_4], PhCl and $P(OMe)_3$ following irradiation at 530 nm for 1 h. Assignments: $P(OMe)_3$, δ = 141.6 ppm; Ph_3PO, δ = 26.8 ppm; $PhPO(OMe)_2$, δ = 21.4 ppm. Ph_3PO was added after the reaction was completed. Yield of $PhPO(OMe)_3$: 13%.

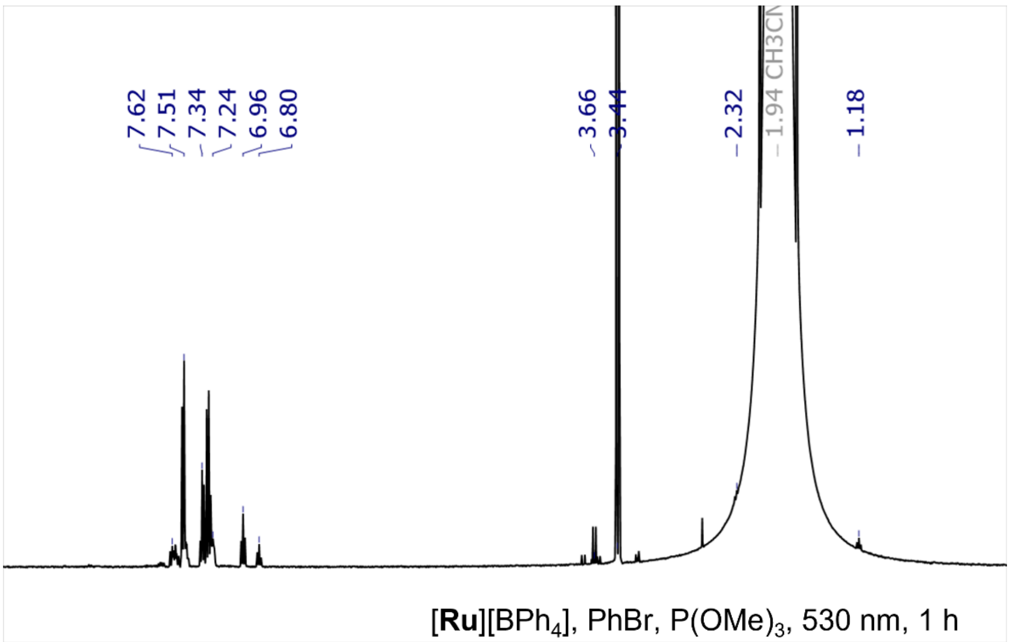

Figure S31: ^{1}H NMR spectrum of the reaction between [Ru][BPh_4], PhBr and $P(OMe)_3$ following irradiation at 530 nm for 1 h. Assignments: $[BPh_4]^-$, δ = 7.24, 6.96 and 6.80 ppm; PhBr, δ = 7.51, 7.34-7.24 ppm; Ph_3PO, δ = 7.62 ppm; $P(OMe)_3$, δ = 3.44 ppm; $PhPO(OMe)_2$, δ = 3.66 ppm. Ph_3PO was added after the reaction was completed.

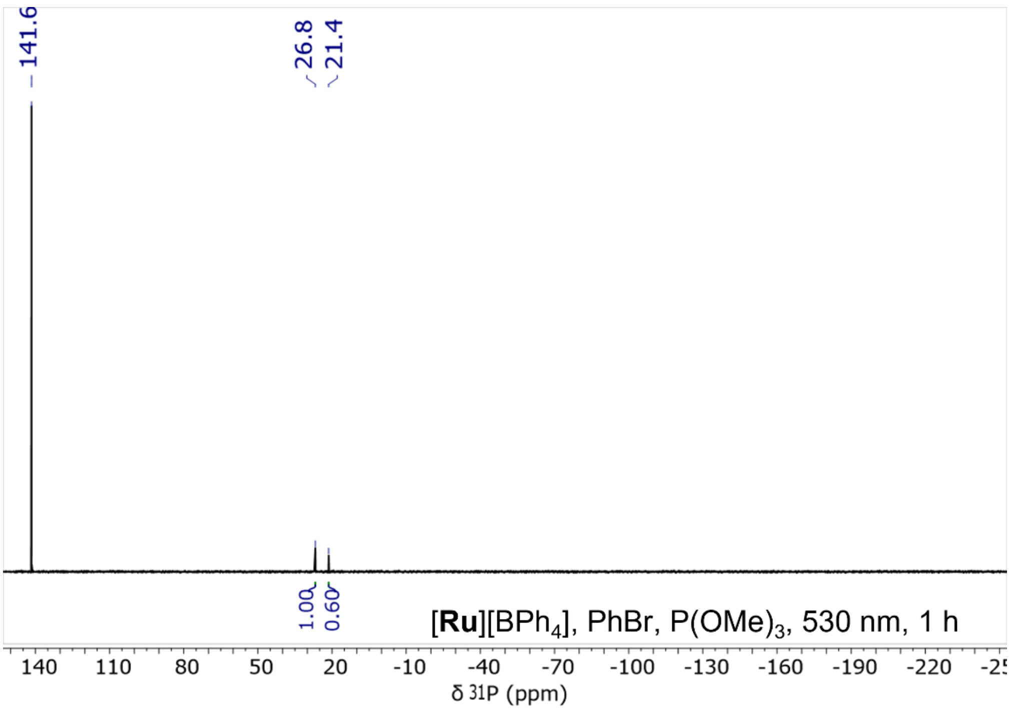

Figure S32: $^{31}P\{^{1}H\}$ NMR spectrum of the reaction between [Ru][BPh_4], PhBr and $P(OMe)_3$ following irradiation at 530 nm for 1 h. Assignments: $P(OMe)_3$, δ = 141.6 ppm; Ph_3PO, δ = 26.8 ppm; $PhPO(OMe)_2$, δ = 21.4 ppm. Ph_3PO was added after the reaction was completed. Yield of $PhPO(OMe)_2$: 60%.

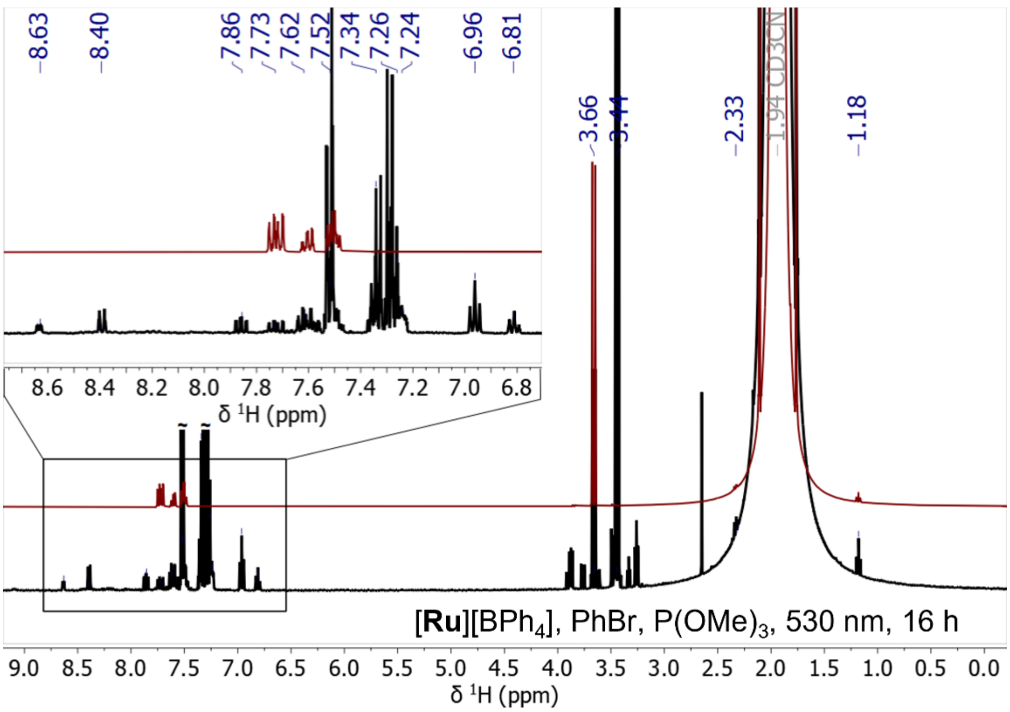

Figure S33: ^{1}H NMR spectrum of the reaction between [Ru][BPh_4], PhBr and $P(OMe)_3$ following irradiation at 530 nm for 16 h. Assignments: $[BPh_4]^-$, δ = 7.24, 6.96 and 6.81 ppm; $[Ru(bipy)_3]^{2+}$, 8.63, 8.40, 7.86 and 7.62 ppm; PhBr, δ = 7.52, 7.34-7.26 ppm; Ph_3PO, δ = 7.62 ppm; $P(OMe)_3$, δ = 3.44 ppm; $PhPO(OMe)_2$, δ = 7.73 and 3.66 ppm. The expansion shows the aromatic region in more detail. Ph_3PO was added after the reaction was completed. Overlaid in maroon is the ^{1}H NMR spectrum of commercially available $PhPO(OMe)_2$.

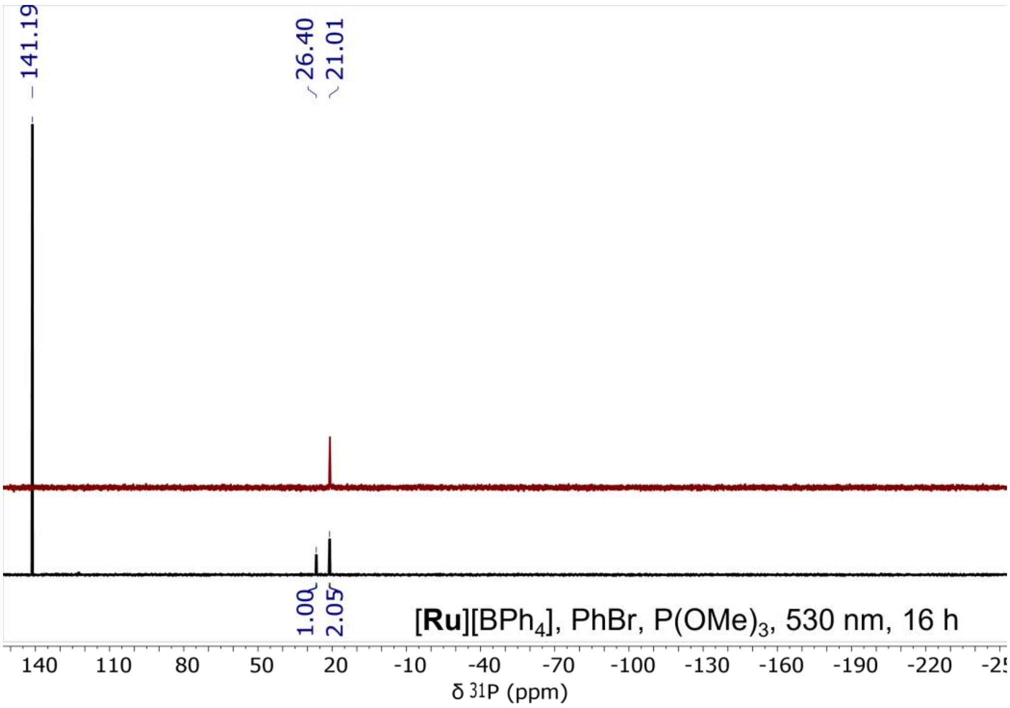

***Figure S34:** $^{31}P\{^{1}H\}$ NMR spectrum of the reaction between [Ru][BPh$_4$], PhBr and P(OMe)$_3$ following irradiation at 530 nm for 16 h. Assignments: P(OMe)$_3$, δ = 141.2 ppm; Ph$_3$PO, δ = 26.4 ppm; PhPO(OMe)$_2$, 21.0 ppm. Ph$_3$PO was added after the reaction. Yield of PhPO(OMe)$_2$ = 205%. Overlaid in maroon is the ^{31}P NMR spectrum of commercially available PhPO(OMe)$_2$.*

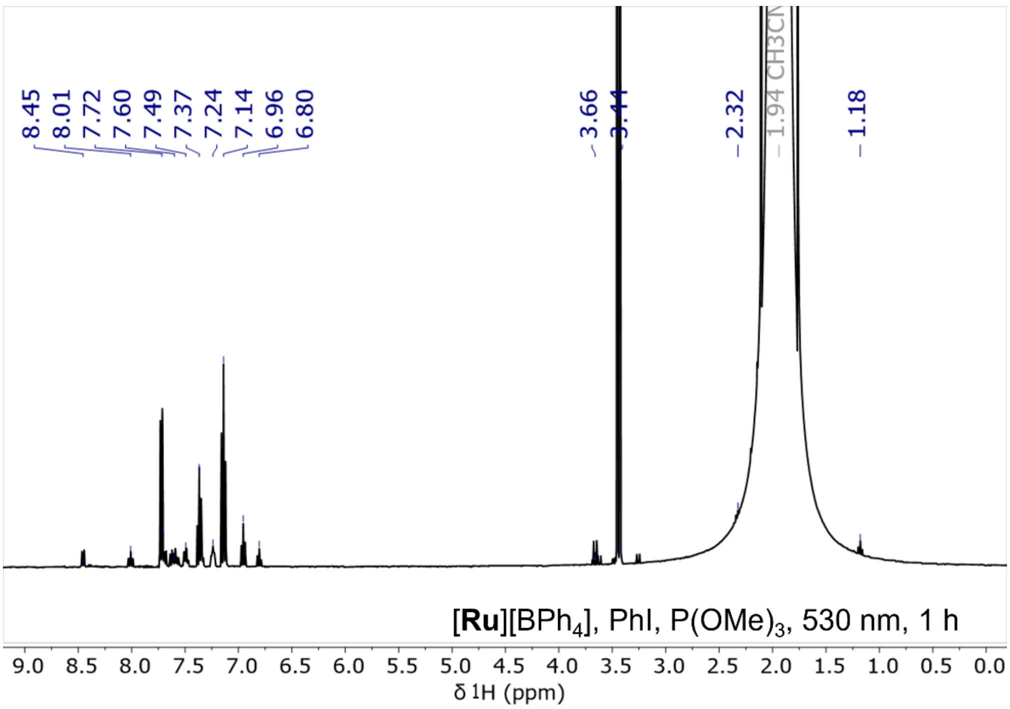

***Figure S35:** ^{1}H NMR spectrum of the reaction between [Ru][BPh$_4$], PhI and P(OMe)$_3$ following irradiation at 530 nm for 1 h. Assignments: [BPh$_4$]$^-$, δ = 7.24, 6.96 and 6.80 ppm; PhI, δ = 7.72, 7.37 and 7.14 ppm; Ph$_3$PO, δ = 7.60 and 7.49 ppm; P(OMe)$_3$, δ = 3.44 ppm; PhPO(OMe)$_2$, δ = 3.66 ppm; [Ru(bipy)$_3$]$^{2+}$, δ = 8.45 and 8.01 ppm. Ph$_3$PO was added after the reaction was completed.*

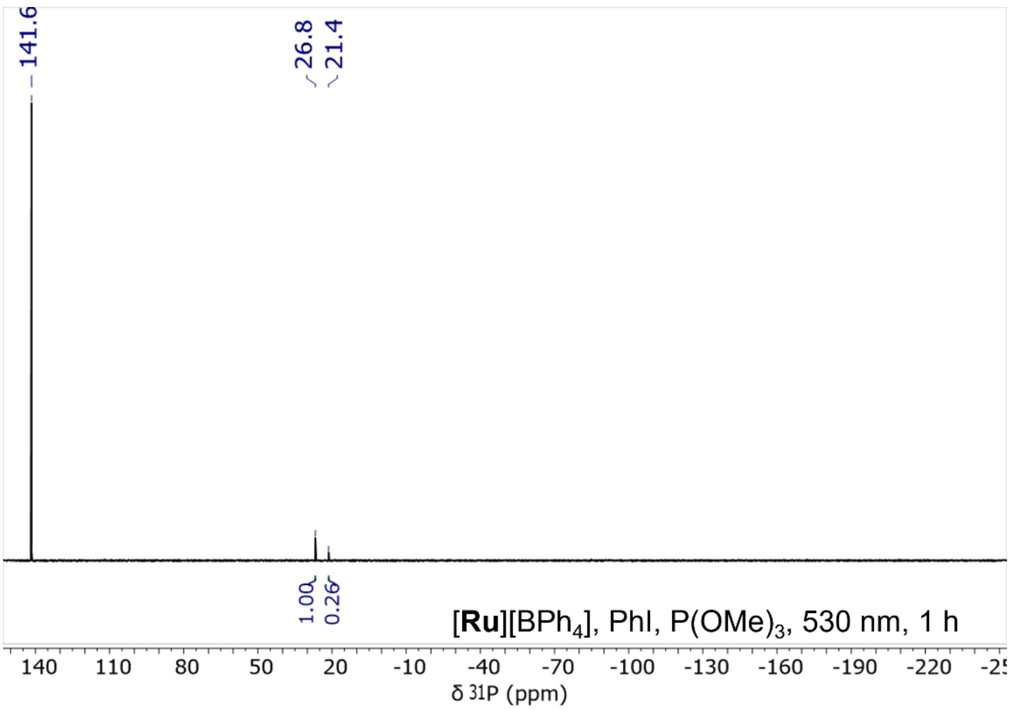

Figure S36: $^{31}P\{^{1}H\}$ NMR spectrum of the reaction between [Ru][BPh₄], PhI and $P(OMe)_3$ following irradiation at 530 nm for 1 h. Assignments: $P(OMe)_3$, δ = 141.6 ppm; Ph_3PO, δ = 26.8 ppm; $PhPO(OMe)_2$, δ = 21.4 ppm. Ph_3PO was added after the reaction was completed. Yield of $PhPO(OMe)_2$: 26%.

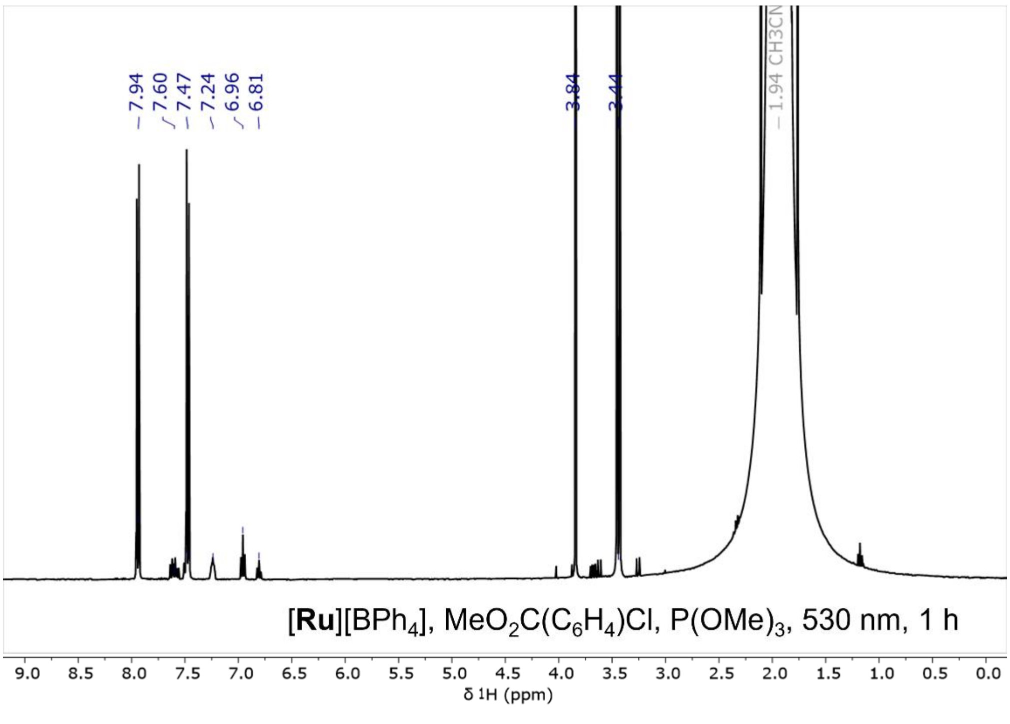

Figure S37: ^{1}H NMR spectrum of the reaction between [Ru][BPh_4], $MeO_2C(C_6H_4)Cl$ and $P(OMe)_3$ following irradiation at 530 nm for 1 h. Assignments: $[BPh_4]^-$, δ = 7.24, 6.96 and 6.81 ppm; $MeO_2C(C_6H_4)Cl$, δ = 7.94, 7.47 and 3.84 ppm; Ph_3PO, δ = 7.60 ppm; $P(OMe)_3$, δ = 3.44 ppm. Ph_3PO was added after the reaction was completed.

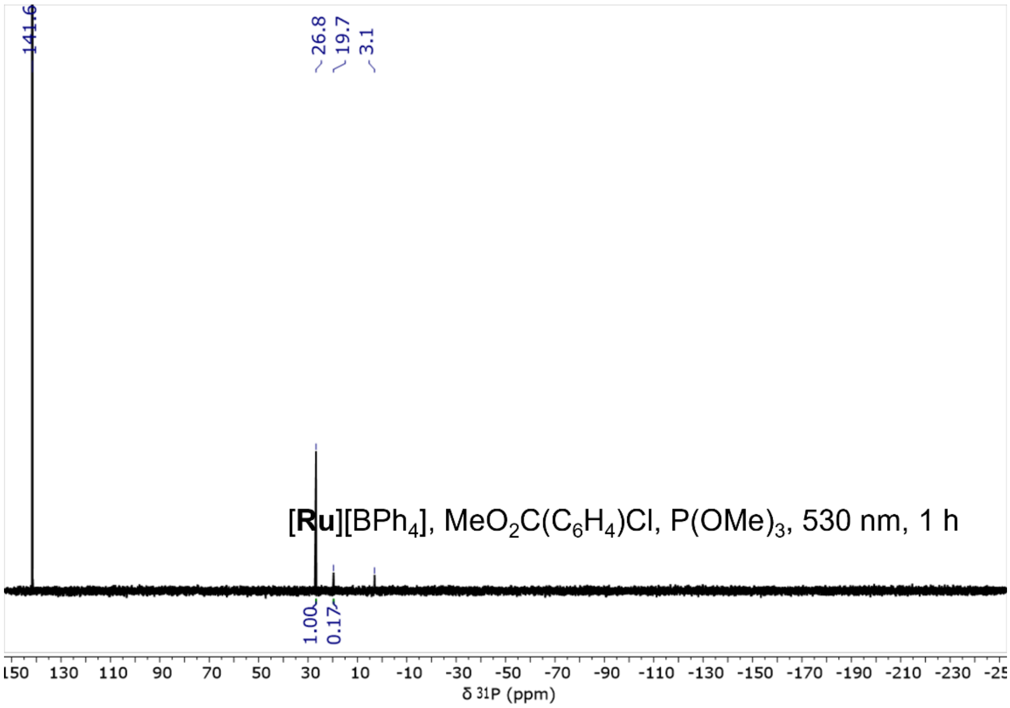

Figure S38: $^{31}P\{^1H\}$ NMR spectrum of the reaction between [Ru][BPh$_4$], $MeO_2C(C_6H_4)Cl$ and $P(OMe)_3$ following irradiation at 530 nm for 1 h. Assignments: $P(OMe)_3$, δ = 141.6 ppm; Ph_3PO, δ = 26.8 ppm; $MeO_2C(C_6H_4)PO(OMe)_2$, δ = 19.7 ppm. Ph_3PO was added after the reaction was completed. Yield of MeO_2-$C(C_6H_4)PO(OMe)_2$ = 17%.

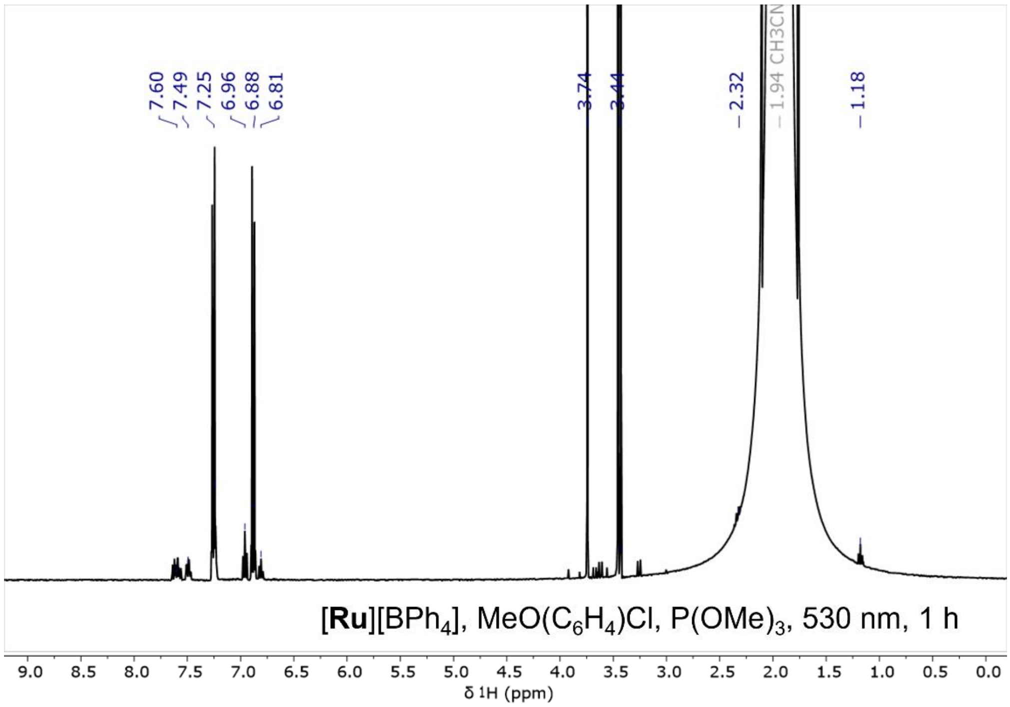

Figure S39: ^1H NMR spectrum of the reaction between [Ru][BPh$_4$], $MeO(C_6H_4)Cl$ and $P(OMe)_3$ following irradiation at 530 nm for 1 h. Assignments: $[BPh_4]^-$, 6.96 and 6.81 ppm; $MeO(C_6H_4)Cl$, δ = 7.25, 6.88 and 3.74 ppm; Ph_3PO, δ = 7.60 and 7.49 ppm; $P(OMe)_3$, 3.44 ppm. Ph_3PO was added after the reaction was completed.

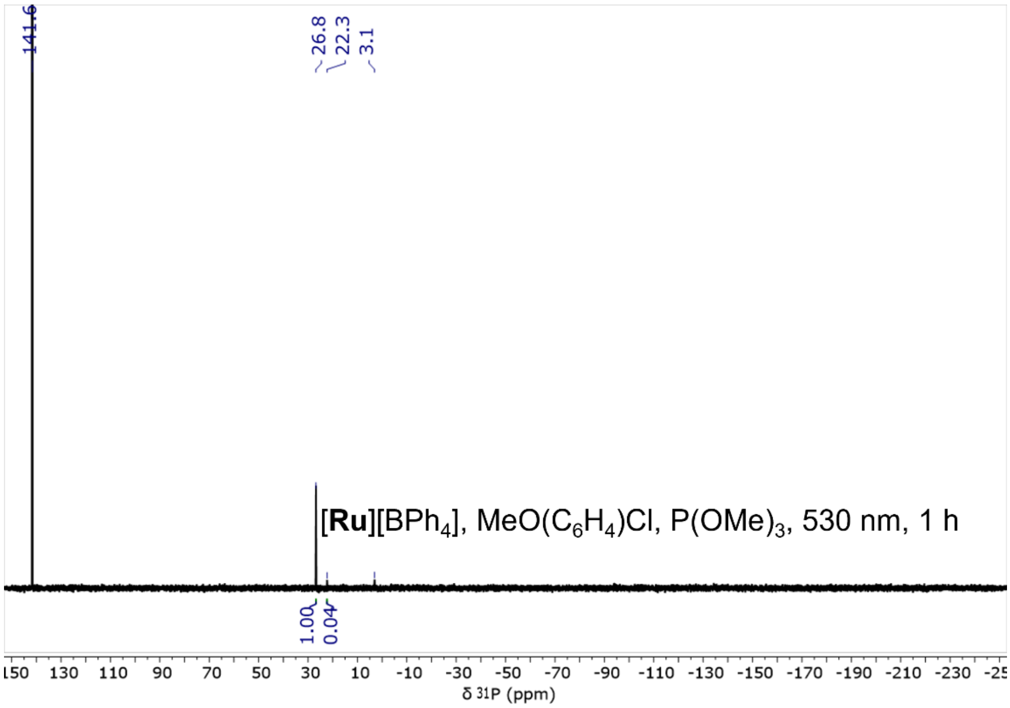

Figure S40: $^{31}P\{^{1}H\}$ NMR spectrum of the reaction between [Ru][BPh_4], MeO(C_6H_4) and $P(OMe)_3$ following irradiation at 530 nm for 1 h. Assignments: $P(OMe)_3$, δ = 141.6 ppm; Ph_3PO, δ = 26.8 ppm; MeO(C_6H_4)PO$(OMe)_2$, δ = 22.3 ppm. Ph_3PO was added after the reaction was completed. Yield of MeO(C_6H_4)PO$(OMe)_2$ = 4%.

3.3 Reduction chemistry of [Ru]Cl_2

To determine whether [**Ru**]Cl_2 could perform similar aryl halide reduction chemistry, solutions containing [**Ru**]Cl_2, PhCl, PhBr or PhI and B_2pin_2 were irradiated with light of 530 or 455 nm for 1 h (see Figure S41 to Figure S49). We chose to use this radical trap as unlike $P(OMe)_3$ it did not appear to react with [**Ru**]Cl_2. Similar products to those observed in the photostability study were detected (arising from the decomposition of [**Ru**]Cl_2 and from the reaction of [**Ru**]Cl_2 with B_2pin_2). However, only in the case of PhI were ^1H resonances consistent with PhBpin (the product of phenyl radical trapping by B_2pin_2) observed. In this case, the amount generated was too small to be observed by $^{11}B\{^1H\}$ NMR, nor was it significant enough to be quantified by ^1H NMR. No significant difference was observed in reactivity at the two different wavelengths.

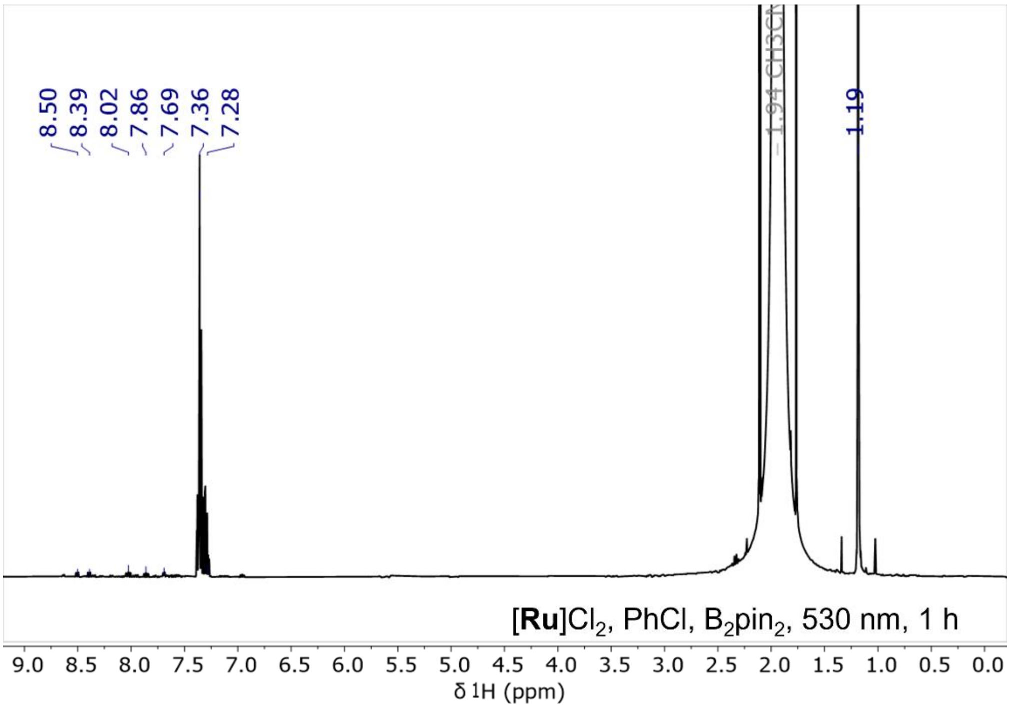

***Figure S41:** ^1H NMR spectrum of the reaction between [Ru]Cl_2, PhCl and B_2pin_2 following irradiation at 530 nm for 1 h. Assignments: PhCl, δ =7.36-7.28 ppm; $[Ru(bipy)_3]^{2+}$, δ = 8.50, 8.02 and 7.69 ppm; B_2pin_2, δ = 1.19 ppm.*

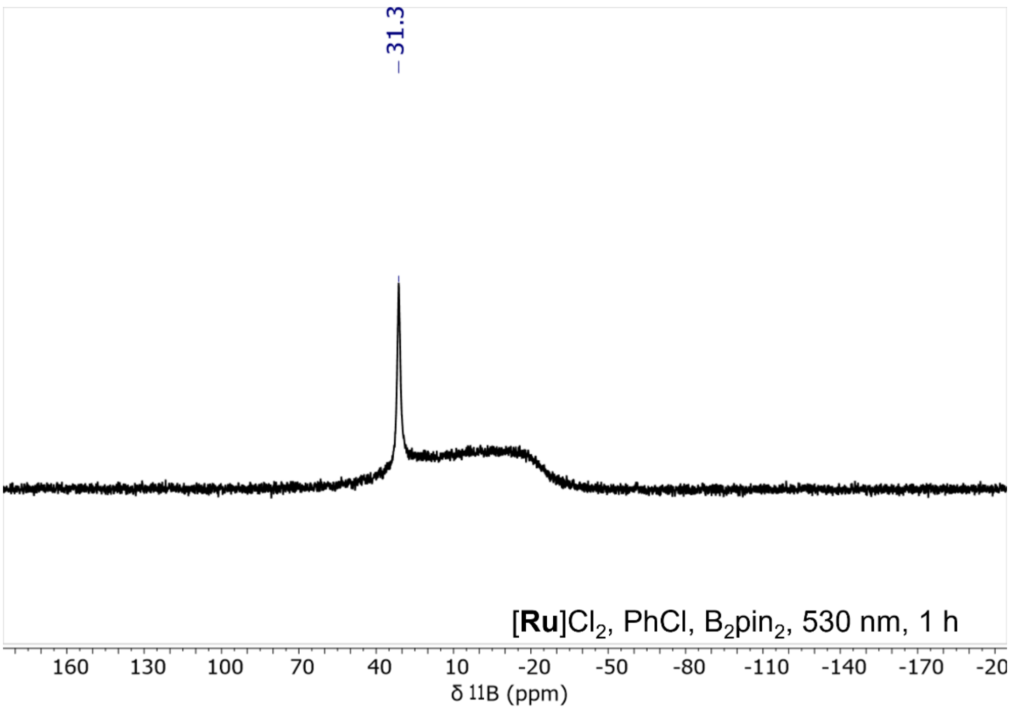

Figure S42: $^{11}B\{^{1}H\}$ NMR spectrum of the reaction between [Ru]Cl_2, PhCl and B_2pin_2 following irradiation at 530 nm for 1 h. Assignment: B_2pin_2, δ = 31.3 ppm.

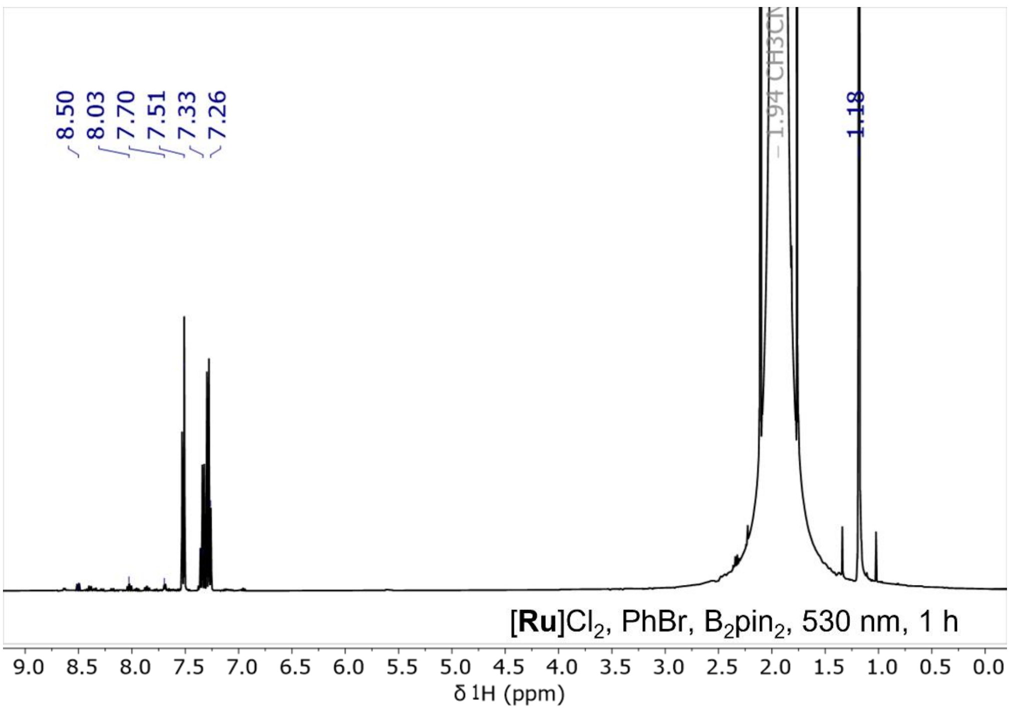

Figure S43: ^{1}H NMR spectrum of the reaction between [Ru]Cl_2, PhBr and B_2pin_2 following irradiation at 530 nm for 1 h. Assignments: PhBr, δ = 7.51, 7.33-7.26 ppm; $[Ru(bipy)_3]^{2+}$, δ = 8.50, 8.03 and 7.70 ppm; B_2pin_2, δ = 1.18 ppm.

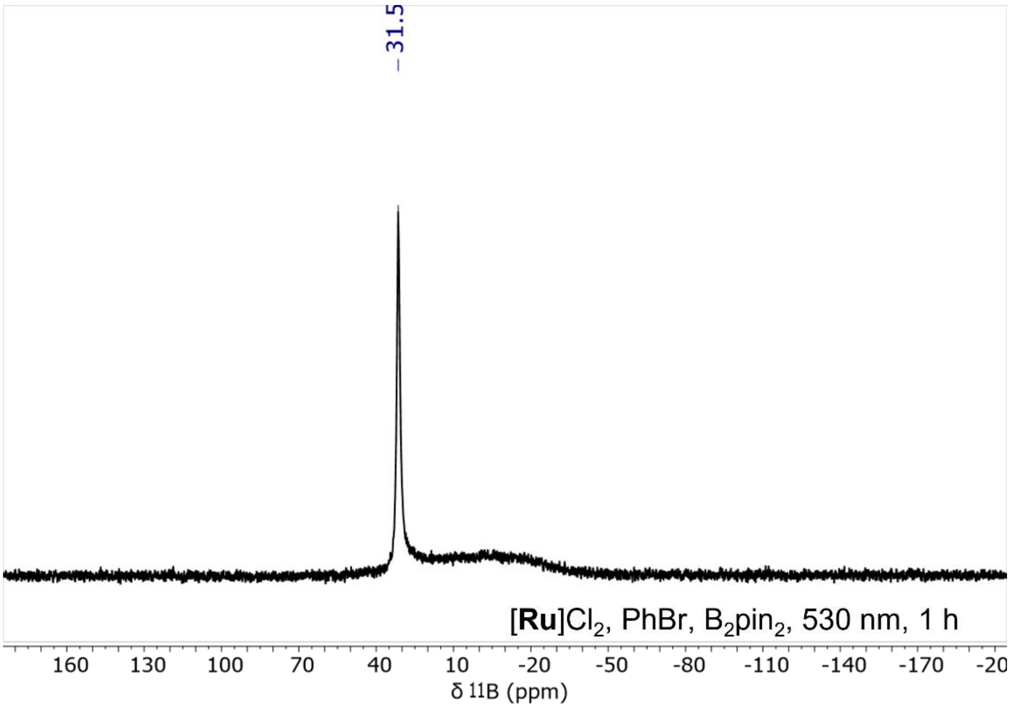

Figure S44: $^{11}B\{^1H\}$ NMR spectrum of the reaction between [Ru]Cl$_2$, PhBr and B$_2$pin$_2$ following irradiation at 530 nm for 1 h. Assignment: B$_2$pin$_2$, δ = 31.5 ppm.

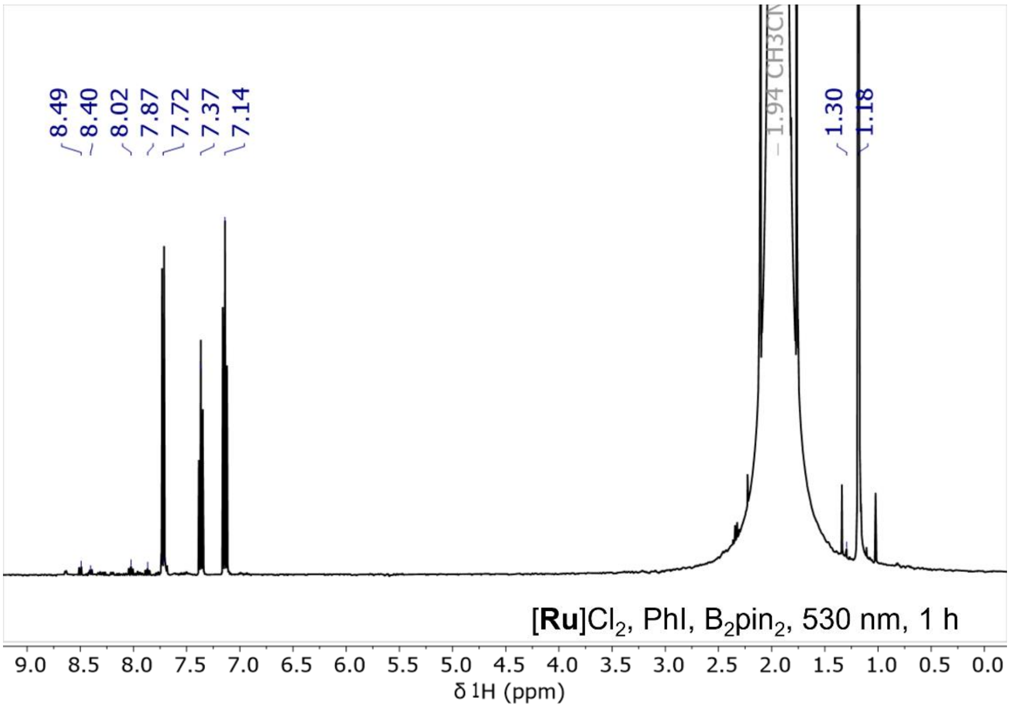

Figure S45: ^1H NMR spectrum of the reaction between [Ru]Cl$_2$, PhI and B$_2$pin$_2$ following irradiation at 530 nm for 1 h. Assignments: PhI, δ = 7.72, 7.37 and 7.14 ppm; [Ru(bipy)$_3$]$^{2+}$, δ = 8.49 and 8.02 ppm; B$_2$pin$_2$, δ = 1.18 ppm; PhBpin, δ = 1.30 ppm. PhBpin conversion was too low to measure reliably.

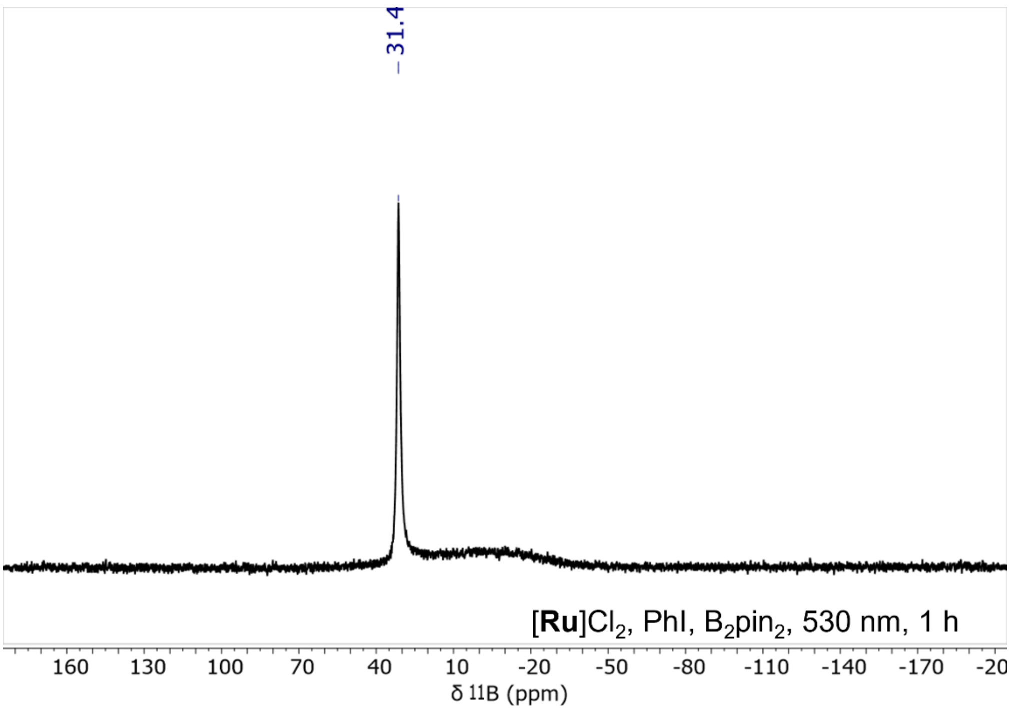

Figure S46:** ***^{11}B{^{1}H} NMR spectrum of the reaction between [Ru]Cl$_2$, PhI and B$_2$pin$_2$ following irradiation at 530 nm for 1 h. Assignment: B$_2$pin$_2$, δ = 31.4 ppm.

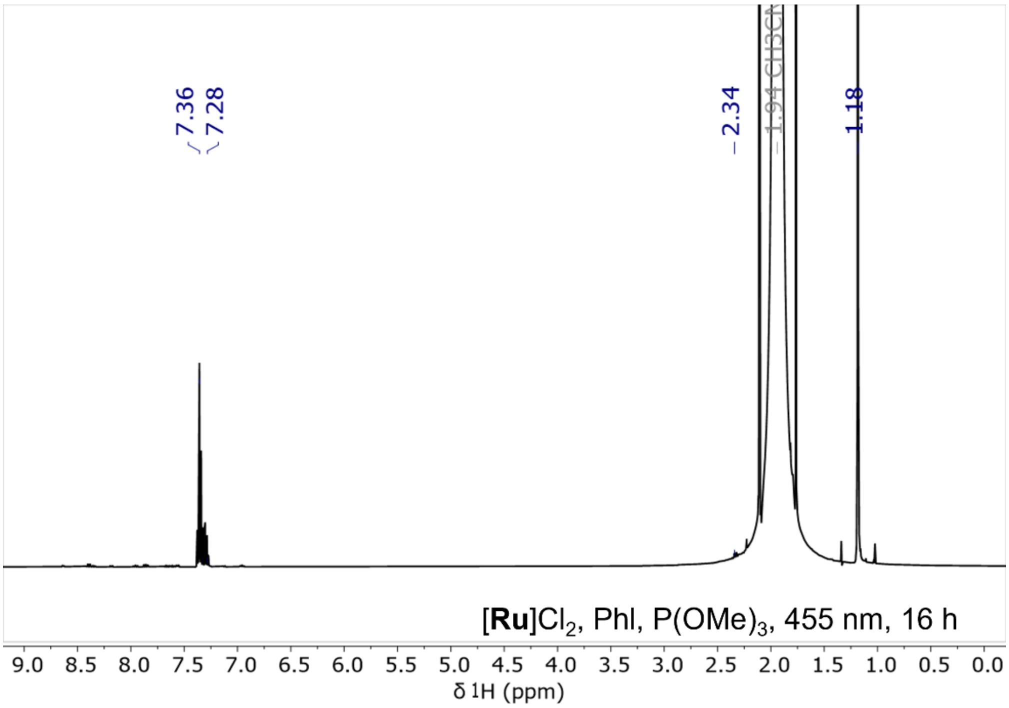

***Figure S47:** ^{1}H NMR spectrum of the reaction between [Ru]Cl$_2$, PhCl and B$_2$pin$_2$ following irradiation at 455 nm for 1 h. Assignments: PhCl, δ = 7.36-7.28 ppm; B$_2$pin$_2$, 1.18 ppm.*

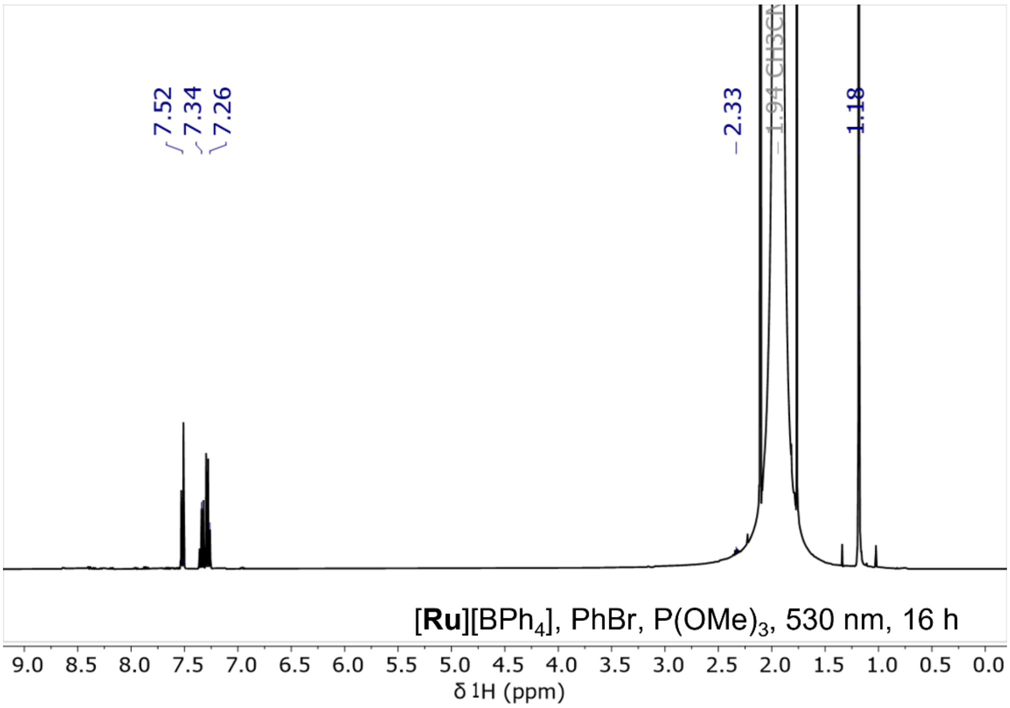

Figure S48: [1]H NMR spectrum of the reaction between [Ru]Cl_2, PhBr and B_2pin_2 following irradiation at 455 nm for 1 h. Assignments: PhBr, δ = 7.52, 7.34-7.26 ppm; B_2pin_2, 1.18 ppm.

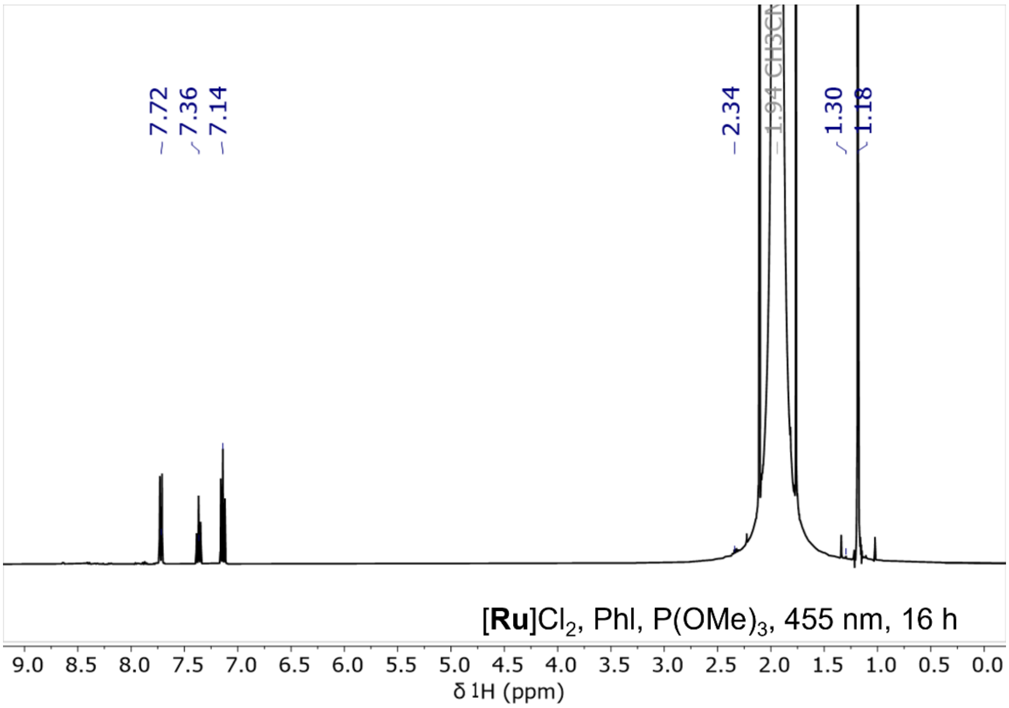

Figure S49: [1]H NMR spectrum of the reaction between [Ru]Cl_2, PhI and B_2pin_2 following irradiation at 455 nm for 1 h. Assignments: PhI, δ = 7.72, 7.36 and 7.14 ppm; B_2pin_2, δ = 1.18 ppm; PhBpin, δ = 1.30 ppm. PhBpin conversion was too low to measure reliably.

4 Crystallographic information

Crystallographic data were collected at 150 K, on the SuperNova Dual diffractometer at the University of Oxford ([**Ru**][BPh_4]·THF) or the Xcalibur EosS2 diffractometer at the University of Bath ([**Ru**][BPh_4]·MeCN). Structures were solved and refined with Olex2 using the ShelXL plugin.[4] CCDC deposition numbers 2290574 ([**Ru**][BPh_4]·THF) and 2290732 ([**Ru**][BPh_4]·MeCN) contain the supplementary crystallographic information for this paper. These can be obtained free of charge from the Cambridge Crystallographic Data Centre.

4.1 XRD data for [Ru][BPh_4]

Tables S1 and S2 contain collected bond distance data as averages and ranges, respectively, for [**Ru**][BPh_4]·THF and [**Ru**][BPh_4]·MeCN, along with bond information for some other compounds containing the $[Ru(bipy)_3]^{n+}$ unit deposited in the CCDC. The numbering system used in the table is illustrated in Figure S50, and is different to the crystallographic atomic numbering. Note that no standard deviations could be calculated for the averaged bond distances due to the small sample sizes (max. 6). The literature compounds selected for comparison were limited to those with discrete, well-defined counter ions, to eliminate uncertainty in oxidation state assignment. See the MS and Figure S50 for discussion and a visual representation of the differences in bond distances between the bipy ligands, respectively. No significant differences were observed between the Ru-N(bipy) bond distances in [**Ru**][BPh_4]·THF and the other complexes considered, despite the oxidation to Ru^{3+} in [**Ru**]$^{3+}$,[5] and reduction of the bipy ligands in [**Ru**]$^{+}$ and [**Ru**]^{0}.[6] It has previously been suggested that this stems from the π-backbonding reducing in strength upon oxidation of Ru^{2+} to Ru^{3+}, thus counteracting the increase in electrostatic interactions. Similarly, addition of an electron to a bipy ligand reduces backbonding from Ru.

Table S1: Compiled average bond distance values from a series of different solid-state molecular structures containing [Ru(bipy)3]n+ (n = 3, 2, 1, 0). The numbering scheme for the bipy ligands is shown in Figure S50.

	Selected bond distances (/Å):							
Complex	N1-C6	C6-C5	C5-C4	C4-C3	C3-C2	N1-C2	C2-C2′	Ru-N1
[a]$[Ru(bipy)_3][PF_6]_3$	1.353	1.379	1.389	1.381	1.389	1.360	1.450	2.057
[b]$[Ru(bipy)_3][PF_6]_2$	1.348	1.372	1.370	1.385	1.376	1.353	1.475	2.056
[**Ru**][BPh_4]·THF: bipy^0	1.347	1.383	1.380	1.381	1.391	1.362	1.469	2.0540
[**Ru**][BPh_4]·THF: bipy^{1-}	1.347	1.379	**1.404**	**1.364**	1.421	**1.394**	**1.419**	2.0545
[**Ru**][BPh_4]·MeCN:	1.345	1.373	1.382	1.373	1.398	1.371	1.446	2.052
[c]$[Ru(bipy)_3]^0$	1.359	1.368	1.402	1.372	1.412	1.383	1.440	2.046

[a]Data from reference 5. [b]Data from reference 7. [c]Data from reference 6. To compile this table, the bond distances of each bipy ligand were given as a range. The only structure that exhibited consistently statistically different bond distances between its bipy ligands was [**Ru**][BPh_4]·THF. Bond distances highlighted in **red** are statistically longer, while those highlighted in **blue** are statistically shorter than equivalent others in the same complex. For an indication of the standard deviations used to calculate the statistical differences, see Table S2.

Table S2: Compiled bond distance ranges from a series of different solid-state molecular structures containing [Ru(bipy)3]n+ (n = 3, 2, 1, 0). The numbering scheme for the bipy ligands is shown in Figure S50.

Complex	Selected bond distances (/Å): N1-C6	C6-C5	C5-C4	C4-C3	C3-C2	N1-C2	C2-C2′	Ru-N1
[a][Ru(bipy)$_3$][PF$_6$]$_3$	1.353(5)	1.379(6)	1.389(6)	1.381(6)	1.389(5)	1.360(5)	1.450(7)	2.057(3)
[b][Ru(bipy)$_3$][PF$_6$]$_2$	1.338(6)-1.361(5)	1.365(6)-1.376(7)	1.356(7)-1.389(7)	1.376(8)-1.403(7)	1.367(7)-1.399(6)	1.336(5)-1.365(5)	1.470(6)-1.478(5)	2.058(4)-2.067(4)
[**Ru**][BPh$_4$]·THF: bipy^0	1.346(2)-1.349(2)	1.381(3)-1.399(3)	1.378(3)-1.383(3)	1.377(3)-1.384(3)	1.389(2)-1.394(3)	1.358(2)-1.364(2)	1.467(3)-1.471(2)	2.0497(13)-2.0568(14)
[**Ru**][BPh$_4$]·THF: bipy^{1-}	1.346(2)-1.347(2)	1.378(3)-1.379(3)	**1.402(3)-1.405(3)**	**1.363(3)-1.364(3)**	1.419(3)-1.423(3)	**1.392(2)-1.395(2)**	**1.419(3)**	2.0489(14)-2.0600(14)
[**Ru**][BPh$_4$]·MeCN:	1.338(3)-1.353(3)	1.371(4)-1.379(4)	1.375(4)-1.392(4)	1.368(4)-1.381(4)	1.384(4)-1.408(4)	1.362(3)-1.382(3)	1.434(4)-1.465(3)	2.045(2)-2.060(2)
[c][Ru(bipy)$_3$]^0	1.355(4)-1.362(4)	1.360(4)-1.375(4)	1.394(5)-1.415(5)	1.367(4)-1.378(4)	1.405(4)-1.417(4)	1.380(3)-1.385(4)	1.431(5)-1.448(4)	2.041(2)-2.059(2)

[a]Data from reference 5. [b]Data from reference 7. [c]Data from reference 6. To compile this table, the bond distances of each bipy ligand were given as a range. The only structure that exhibited consistently statistically different bond distances between its bipy ligands was [**Ru**][BPh$_4$]·THF. Bond distances highlighted in **red** are statistically longer, while those highlighted in **blue** are statistically shorter than equivalent others in the same complex.

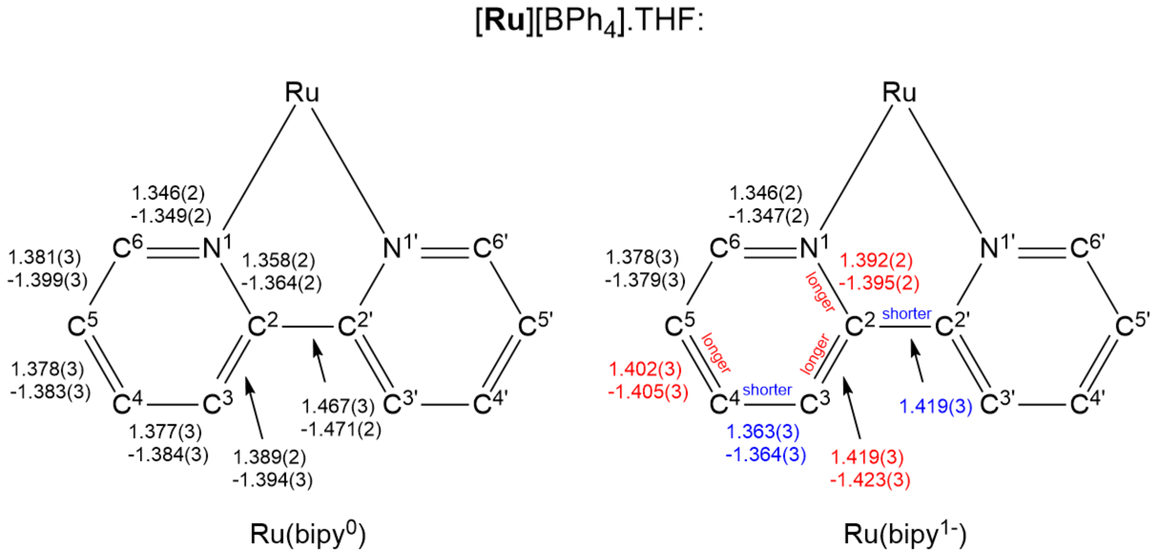

Figure S50: Atomic numbering of the bipy ligands used to complete Table S1: Compiled average bond distance values from a series of different solid-state molecular structures containing [Ru(bipy)3]n+ (n = 3, 2, 1, 0). The numbering scheme for the bipy ligands is shown in Figure S50.

Complex	Selected bond distances (/Å): N1-C6	C6-C5	C5-C4	C4-C3	C3-C2	N1-C2	C2-C2′	Ru-N1
[a][Ru(bipy)$_3$][PF6]$_3$	1.353	1.379	1.389	1.381	1.389	1.360	1.450	2.057
[b][Ru(bipy)$_3$][PF6]$_2$	1.348	1.372	1.370	1.385	1.376	1.353	1.475	2.056
[**Ru**][BPh4]·THF: bipy0	1.347	1.383	1.380	1.381	1.391	1.362	1.469	2.0540
[**Ru**][BPh4]·THF: bipy1⁻	1.347	1.379	**1.404**	**1.364**	1.421	**1.394**	**1.419**	2.0545
[**Ru**][BPh4]·MeCN :	1.345	1.373	1.382	1.373	1.398	1.371	1.446	2.052
[c][Ru(bipy)$_3$]^0	1.359	1.368	1.402	1.372	1.412	1.383	1.440	2.046

[aData] from reference 5. [bData] from reference 7. [cData] from reference 6. To compile this table, the bond distances of each bipy ligand were given as a range. The only structure that exhibited consistently statistically different bond distances between its bipy ligands was [**Ru**][BPh4]·THF. Bond distances highlighted in **red** are statistically longer, while those highlighted in **blue** are statistically shorter than equivalent others in the same complex. For an indication of the standard deviations used to calculate the statistical differences, see Table S2.

4.2 Crystallographic collection data and full bond information for [Ru][BPh_4]·THF

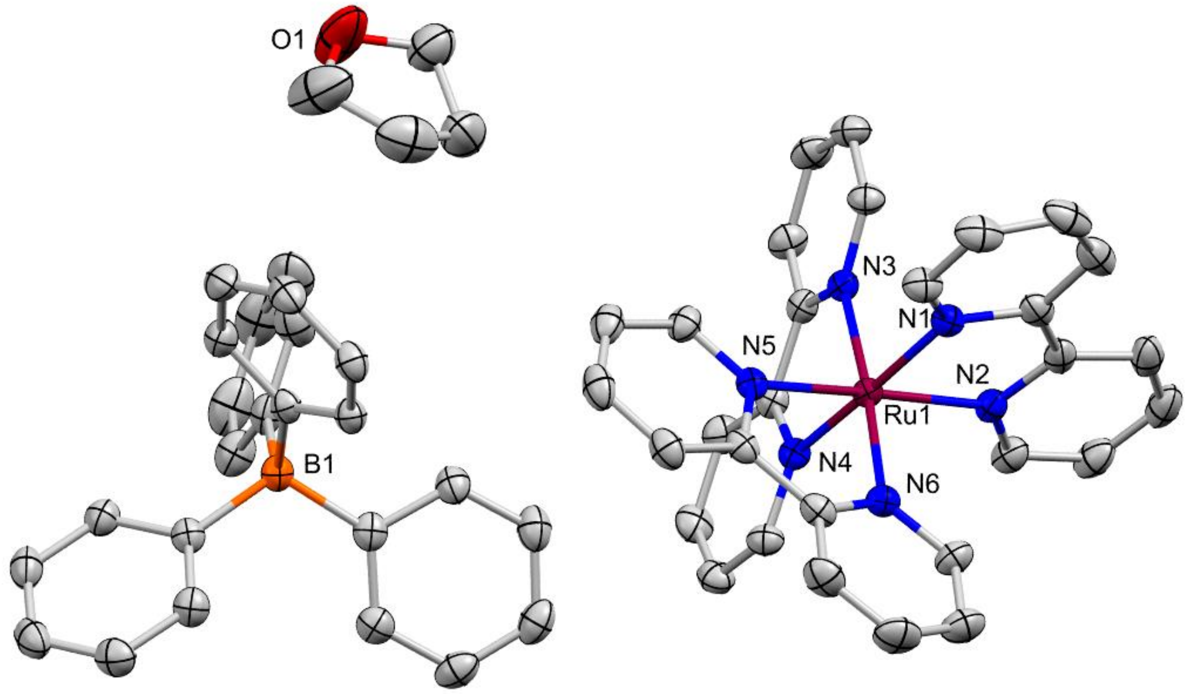

Figure S51: Solid-state molecular structure of [Ru][BPh_4]·THF. Ellipsoids drawn at 50% probability. H atoms omitted for clarity. Atom colours: Ru, burgundy; N, blue; B, orange; O, red; C, grey.

Table S3: Crystallographic data and structure refinement details for [Ru][BPh_4]·THF

Empirical formula	**$C_{58}H_{48}BN_6ORu$**
Formula weight	960.93
Temperature/K	150.15
Crystal system	monoclinic
Space group	$P2_1/c$
a/Å	12.20192(15)
b/Å	28.9704(4)
c/Å	13.67518(16)
α/°	90
β/°	99.9543(12)
γ/°	90
Volume/Å^3	4761.33(11)
Z	4
ρ_{calc}g/cm^3	1.341
μ/mm^{-1}	3.035
F(000)	1996.0
Crystal size/mm^3	0.2 × 0.2 × 0.1
Radiation	Cu Kα (λ = 1.54184)
2Θ range for data collection/°	7.238 to 152.742
Index ranges	$-15 \leq h \leq 15$, $-36 \leq k \leq 35$, $-15 \leq l \leq 17$
Reflections collected	38786
Independent reflections	9872 [R_{int} = 0.0358, R_{sigma} = 0.0289]
Data/restraints/parameters	9872/0/604
Goodness-of-fit on F^2	1.034
Final R indexes [I>=2σ (I)]	R_1 = 0.0270, wR_2 = 0.0659
Final R indexes [all data]	R_1 = 0.0326, wR_2 = 0.0693
Largest diff. peak/hole / e Å^{-3}	0.59/-0.49

Table S4: Tabulated bond distances in [Ru][BPh$_4$]·THF

Atom 1	Atom 2	Bond Distance (Å)	Atom 1	Atom 2	Bond Distance (Å)
Ru1	N1	2.0489(14)	C17	C18	1.384(3)
Ru1	N2	2.0600(14)	C18	C19	1.379(3)
Ru1	N3	2.0568(14)	C19	C20	1.381(2)
Ru1	N4	2.0552(14)	C21	C22	1.385(3)
Ru1	N5	2.0497(13)	C22	C23	1.379(3)
Ru1	N6	2.0542(14)	C23	C24	1.377(3)
O1	C55	1.405(4)	C24	C25	1.389(2)
O1	C58	1.398(3)	C25	C26	1.467(3)
N1	C1	1.347(2)	C26	C27	1.394(3)
N1	C5	1.395(2)	C27	C28	1.381(3)
N2	C6	1.392(2)	C28	C29	1.378(3)
N2	C10	1.346(2)	C29	C30	1.382(3)
N3	C11	1.345(2)	C31	C32	1.399(3)
N3	C15	1.361(2)	C31	C36	1.400(3)
N4	C16	1.363(2)	C32	C33	1.393(3)
N4	C20	1.346(2)	C33	C34	1.379(4)
N5	C21	1.346(2)	C34	C35	1.377(4)
N5	C25	1.364(2)	C35	C36	1.390(3)
N6	C26	1.358(2)	C37	C38	1.406(3)
N6	C30	1.349(2)	C37	C42	1.403(3)
B1	C31	1.643(3)	C38	C39	1.396(3)
B1	C37	1.645(2)	C39	C40	1.381(3)
B1	C43	1.645(3)	C40	C41	1.383(3)
B1	C49	1.648(3)	C41	C42	1.391(3)
C1	C2	1.378(3)	C43	C44	1.398(3)
C2	C3	1.405(3)	C43	C48	1.410(2)
C3	C4	1.363(3)	C44	C45	1.402(3)
C4	C5	1.419(3)	C45	C46	1.377(3)
C5	C6	1.419(3)	C46	C47	1.389(3)
C6	C7	1.423(3)	C47	C48	1.392(3)
C7	C8	1.364(3)	C49	C50	1.402(2)
C8	C9	1.402(3)	C49	C54	1.410(2)
C9	C10	1.379(3)	C50	C51	1.398(3)
C11	C12	1.384(3)	C51	C52	1.386(3)
C12	C13	1.383(3)	C52	C53	1.388(3)
C13	C14	1.381(3)	C53	C54	1.391(3)
C14	C15	1.391(2)	C55	C56	1.519(4)
C15	C16	1.471(2)	C56	C57	1.508(4)
C16	C17	1.391(2)	C57	C58	1.498(4)

Table S5: Tabulated bond angles in [Ru][BPh$_4$]·THF

Atom 1	Atom 2	Atom 3	Angle (˚)	Atom 1	Atom 2	Atom 3	Angle (˚)
N1	Ru1	N2	79.59(6)	N3	C15	C16	114.57(14)
N1	Ru1	N3	95.15(5)	C14	C15	C16	123.84(16)
N1	Ru1	N4	172.44(6)	N4	C16	C15	114.52(14)
N1	Ru1	N5	96.22(6)	N4	C16	C17	121.25(16)
N1	Ru1	N6	87.41(5)	C17	C16	C15	124.17(16)
N3	Ru1	N2	87.46(5)	C18	C17	C16	119.68(17)
N4	Ru1	N2	95.81(6)	C19	C18	C17	118.91(17)
N4	Ru1	N3	78.57(5)	C18	C19	C20	119.13(17)
N5	Ru1	N2	173.59(6)	N4	C20	C19	122.80(17)
N5	Ru1	N3	97.80(5)	N5	C21	C22	122.31(18)
N5	Ru1	N4	88.85(5)	C23	C22	C21	119.26(18)
N5	Ru1	N6	78.92(6)	C24	C23	C22	119.26(17)
N6	Ru1	N2	95.96(6)	C23	C24	C25	119.34(18)

N6	Ru1	N3	176.06(5)	N5	C25	C24	121.59(17)
N6	Ru1	N4	99.09(5)	N5	C25	C26	114.72(14)
C58	O1	C55	110.3(2)	C24	C25	C26	123.69(17)
C1	N1	Ru1	126.70(12)	N6	C26	C25	114.79(15)
C1	N1	C5	118.78(15)	N6	C26	C27	121.29(17)
C5	N1	Ru1	114.51(12)	C27	C26	C25	123.92(17)
C6	N2	Ru1	113.95(11)	C28	C27	C26	119.44(19)
C10	N2	Ru1	126.91(13)	C29	C28	C27	119.22(18)
C10	N2	C6	119.12(15)	C28	C29	C30	119.04(18)
C11	N3	Ru1	125.60(12)	N6	C30	C29	122.59(18)
C11	N3	C15	118.51(15)	C32	C31	B1	121.90(18)
C15	N3	Ru1	115.85(11)	C32	C31	C36	114.77(19)
C16	N4	Ru1	116.00(11)	C36	C31	B1	123.07(18)
C20	N4	Ru1	125.77(12)	C33	C32	C31	122.9(2)
C20	N4	C16	118.21(15)	C34	C33	C32	120.3(2)
C21	N5	Ru1	126.07(12)	C35	C34	C33	118.6(2)
C21	N5	C25	118.23(15)	C34	C35	C36	120.6(2)
C25	N5	Ru1	115.68(11)	C35	C36	C31	122.8(2)
C26	N6	Ru1	115.65(11)	C38	C37	B1	121.32(15)
C30	N6	Ru1	125.74(12)	C42	C37	B1	123.18(16)
C30	N6	C26	118.42(15)	C42	C37	C38	115.22(16)
C31	B1	C37	112.20(14)	C39	C38	C37	122.65(17)
C31	B1	C43	103.97(13)	C40	C39	C38	120.15(19)
C31	B1	C49	111.00(15)	C39	C40	C41	118.89(18)
C37	B1	C43	113.72(15)	C40	C41	C42	120.65(18)
C37	B1	C49	104.59(13)	C41	C42	C37	122.41(18)
C43	B1	C49	111.55(14)	C44	C43	B1	125.83(16)
N1	C1	C2	123.56(18)	C44	C43	C48	115.11(16)
C1	C2	C3	118.16(19)	C48	C43	B1	118.92(16)
C4	C3	C2	119.76(18)	C43	C44	C45	122.48(18)
C3	C4	C5	120.61(19)	C46	C45	C44	120.55(19)
N1	C5	C4	118.93(18)	C45	C46	C47	118.92(18)
N1	C5	C6	115.48(15)	C46	C47	C48	120.01(18)
C6	C5	C4	125.59(17)	C47	C48	C43	122.93(18)
N2	C6	C5	116.05(15)	C50	C49	B1	124.51(15)
N2	C6	C7	118.80(18)	C50	C49	C54	115.12(16)
C5	C6	C7	125.12(18)	C54	C49	B1	120.20(15)
C8	C7	C6	120.7(2)	C51	C50	C49	122.87(17)
C7	C8	C9	119.55(18)	C52	C51	C50	119.99(17)
C10	C9	C8	118.5(2)	C51	C52	C53	119.02(18)
N2	C10	C9	123.30(19)	C52	C53	C54	120.26(18)
N3	C11	C12	122.29(17)	C53	C54	C49	122.72(18)
C13	C12	C11	119.22(17)	O1	C55	C56	107.1(2)
C14	C13	C12	119.15(17)	C57	C56	C55	103.1(2)
C13	C14	C15	119.22(17)	C58	C57	C56	102.4(2)
N3	C15	C14	121.54(16)	O1	C58	C57	107.2(2)

4.3 Crystallographic collection data and full bond information for [Ru][BPh_4]·MeCN

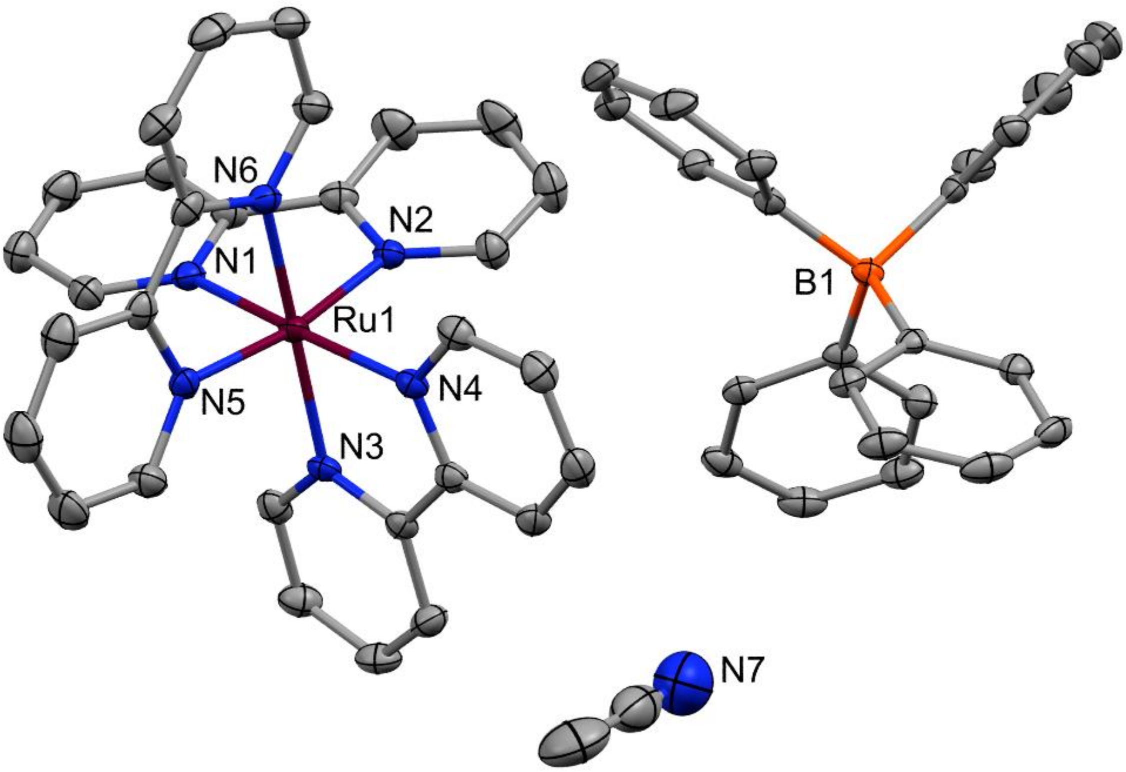

Figure S52: Solid-state molecular structure of [Ru][BPh_4]·MeCN. Ellipsoids drawn at 50% probability. H atoms omitted for clarity. Atom colours: Ru, burgundy; N, blue; B, orange; C, grey.

Table S6: Crystallographic collection data and structure refinement details for [Ru][BPh_4]·MeCN

Empirical formula	$C_{56}H_{47}BN_7Ru$
Formula weight	929.934
Temperature/K	149.9(6)
Crystal system	triclinic
Space group	P-1
a/Å	12.3868(4)
b/Å	13.6724(4)
c/Å	14.1067(5)
α/°	98.518(3)
β/°	108.278(3)
γ/°	96.802(3)
Volume/Å^3	2208.65(14)
Z	2
ρ_{calc}g/cm^3	1.398
μ/mm^{-1}	0.404
F(000)	960.0
Crystal size/mm^3	0.3 × 0.2 × 0.1
Radiation	Mo Kα (λ = 0.71073)
2Θ range for data collection/°	6.02 to 54.96
Index ranges	-15 ≤ h ≤ 16, -17 ≤ k ≤ 17, -17 ≤ l ≤ 17
Reflections collected	19980
Independent reflections	9825 [R_{int} = 0.0358, R_{sigma} = 0.0656]
Data/restraints/parameters	9825/0/587
Goodness-of-fit on F^2	1.047
Final R indexes [I>=2σ (I)]	R_1 = 0.0441, wR_2 = 0.0842
Final R indexes [all data]	R_1 = 0.0604, wR_2 = 0.0912
Largest diff. peak/hole / e Å^{-3}	0.61/-0.81

Table S7: Tabulated bond distances in [Ru][BPh$_4$]·MeCN

Atom 1	Atom 2	Bond Distance (Å)	Atom 1	Atom 2	Bond Distance (Å)
Ru1	N1	2.059(2)	C17	C18	1.374(4)
Ru1	N2	2.048(2)	C18	C19	1.380(4)
Ru1	N3	2.054(2)	C19	C20	1.377(4)
Ru1	N4	2.054(2)	C21	C22	1.369(4)
Ru1	N5	2.044(2)	C22	C23	1.376(4)
Ru1	N6	2.050(2)	C23	C24	1.375(4)
B1	C31	1.641(4)	C24	C25	1.401(4)
B1	C37	1.648(4)	C25	C26	1.442(4)
B1	C43	1.645(4)	C26	C27	1.405(4)
B1	C49	1.639(4)	C27	C28	1.380(4)
N1	C1	1.340(3)	C28	C29	1.375(4)
N1	C5	1.377(3)	C29	C30	1.370(4)
N2	C6	1.381(3)	C31	C32	1.399(4)
N2	C10	1.337(3)	C31	C36	1.402(4)
N3	C11	1.344(3)	C32	C33	1.382(4)
N3	C15	1.362(3)	C33	C34	1.379(4)
N4	C16	1.363(3)	C34	C35	1.380(4)
N4	C20	1.351(3)	C35	C36	1.384(4)
N5	C21	1.350(3)	C37	C38	1.400(3)
N5	C25	1.374(3)	C37	C42	1.404(4)
N6	C26	1.371(3)	C38	C39	1.396(4)
N6	C30	1.349(3)	C39	C40	1.378(4)
N7	C55	1.128(5)	C40	C41	1.384(4)
C1	C2	1.378(4)	C41	C42	1.378(4)
C2	C3	1.391(4)	C43	C44	1.394(4)
C3	C4	1.367(4)	C43	C48	1.402(3)
C4	C5	1.407(4)	C44	C45	1.391(4)
C5	C6	1.432(4)	C45	C46	1.372(4)
C6	C7	1.401(4)	C46	C47	1.376(4)
C7	C8	1.367(4)	C47	C48	1.385(4)
C8	C9	1.386(4)	C49	C50	1.401(4)
C9	C10	1.370(4)	C49	C54	1.400(3)
C11	C12	1.375(4)	C50	C51	1.397(4)
C12	C13	1.385(4)	C51	C52	1.374(4)
C13	C14	1.376(4)	C52	C53	1.381(4)
C14	C15	1.392(4)	C53	C54	1.388(4)
C15	C16	1.463(3)	C55	C56	1.436(6)
C16	C17	1.384(4)			

Table S8: Tabulated bond angles in [Ru][BPh$_4$]·MeCN

Atom 1	Atom 2	Atom 3	Angle (°)	Atom 1	Atom 2	Atom 3	Angle/°
N2	Ru1	N1	79.30(8)	C14	C15	N3	121.0(2)
N3	Ru1	N1	97.59(8)	C16	C15	N3	114.8(2)
N3	Ru1	N2	91.18(8)	C16	C15	C14	124.3(2)
N4	Ru1	N1	172.64(8)	C15	C16	N4	114.5(2)
N4	Ru1	N2	94.47(8)	C17	C16	N4	121.0(2)
N4	Ru1	N3	78.48(8)	C17	C16	C15	124.5(2)
N5	Ru1	N1	94.34(8)	C18	C17	C16	120.4(3)
N5	Ru1	N2	170.96(9)	C19	C18	C17	118.7(3)
N5	Ru1	N3	96.05(8)	C20	C19	C18	119.2(3)
N5	Ru1	N4	92.28(8)	C19	C20	N4	122.7(3)
N6	Ru1	N1	87.92(8)	C22	C21	N5	123.5(3)
N6	Ru1	N2	94.12(8)	C23	C22	C21	119.1(3)
N6	Ru1	N3	172.99(8)	C24	C23	C22	119.1(3)

N6	Ru1	N4	96.51(8)	C25	C24	C23	120.4(3)
N6	Ru1	N5	79.13(9)	C24	C25	N5	120.0(3)
C37	B1	C31	114.0(2)	C26	C25	N5	115.0(2)
C43	B1	C31	105.1(2)	C26	C25	C24	125.0(3)
C43	B1	C37	110.3(2)	C25	C26	N6	115.2(2)
C49	B1	C31	110.9(2)	C27	C26	N6	119.8(3)
C49	B1	C37	105.3(2)	C27	C26	C25	125.0(3)
C49	B1	C43	111.5(2)	C28	C27	C26	119.8(3)
C1	N1	Ru1	127.42(18)	C29	C28	C27	119.8(3)
C5	N1	Ru1	114.34(17)	C30	C29	C28	118.5(3)
C5	N1	C1	118.2(2)	C29	C30	N6	123.5(3)
C6	N2	Ru1	114.57(17)	C32	C31	B1	122.0(2)
C10	N2	Ru1	127.05(18)	C36	C31	B1	123.6(2)
C10	N2	C6	118.2(2)	C36	C31	C32	114.3(2)
C11	N3	Ru1	125.54(18)	C33	C32	C31	123.4(3)
C15	N3	Ru1	116.10(16)	C34	C33	C32	120.0(3)
C15	N3	C11	118.4(2)	C35	C34	C33	118.9(3)
C16	N4	Ru1	116.17(16)	C36	C35	C34	120.0(3)
C20	N4	Ru1	125.76(18)	C35	C36	C31	123.2(3)
C20	N4	C16	118.0(2)	C38	C37	B1	125.3(2)
C21	N5	Ru1	126.68(19)	C42	C37	B1	120.0(2)
C25	N5	Ru1	115.20(17)	C42	C37	C38	114.6(2)
C25	N5	C21	118.0(2)	C39	C38	C37	122.6(3)
C26	N6	Ru1	115.11(17)	C40	C39	C38	120.5(3)
C30	N6	Ru1	126.31(19)	C41	C40	C39	118.5(2)
C30	N6	C26	118.6(2)	C42	C41	C40	120.4(3)
C2	C1	N1	123.6(3)	C41	C42	C37	123.3(2)
C3	C2	C1	118.5(3)	C44	C43	B1	125.1(2)
C4	C3	C2	119.3(3)	C48	C43	B1	119.6(2)
C5	C4	C3	120.2(3)	C48	C43	C44	115.1(2)
C4	C5	N1	120.1(2)	C45	C44	C43	122.5(3)
C6	C5	N1	115.8(2)	C46	C45	C44	120.4(3)
C6	C5	C4	124.1(2)	C47	C46	C45	119.0(3)
C5	C6	N2	115.2(2)	C48	C47	C46	120.1(3)
C7	C6	N2	119.8(2)	C47	C48	C43	122.7(3)
C7	C6	C5	125.0(3)	C50	C49	B1	122.6(2)
C8	C7	C6	120.1(3)	C54	C49	B1	122.3(2)
C9	C8	C7	119.4(3)	C54	C49	C50	115.0(2)
C10	C9	C8	118.6(3)	C51	C50	C49	122.6(3)
C9	C10	N2	123.6(3)	C52	C51	C50	120.0(3)
C12	C11	N3	122.9(3)	C53	C52	C51	119.5(3)
C13	C12	C11	119.0(2)	C54	C53	C52	119.7(3)
C14	C13	C12	118.9(3)	C53	C54	C49	123.2(3)
C15	C14	C13	119.8(3)	C56	C55	N7	179.1(5)

5 References

1 I.S. Weitz, M. Rabinovitz, *J. Chem. Soc. Perkin Trans. 1*, 1993, 117-120

2 S.J. Horsewill, G. Hierlmeier, Z. Farasat, J.P. Barham and D.J. Scott, *ACS Cat.*, 2023, **13**, 9392-9403

3 U. Lennert, P.B. Arockiam, V. Streitferdt, D.J. Scott, C. Rödl, R.M. Gschwind and R. Wolf, *Nature Catal.* 2019, **2**, 1101-1106.

4 a) O.V. Dolomanov, L.J. Bourhis, R.J. Gildea, J.A.K. Howard and H Puschmann, "*Olex2: A complete structure solution, refinement and analysis program"*, *J. Appl. Cryst.*, 2009, **42**, 339-341; b) G. Sheldrick, *"Crystal Structure Refinement with SHELXL", Acta Crystallogr. C*, 2015, **71**, 3-8.

5 M. Biner, H.-B. Bürgi, A. Ludi and C. Röhr, *J. Am. Chem. Soc.,* 1992, **114**, 5197-5203.

6 E.E. Pérez-Cordero, C. Campana and L. Echegoyen, *Angew. Chem. Intl. Ed. Engl.,* 1997, **36**, 137-140.

7 J. Breu, H. Domel and A. Stoll, *Eur. J. Inorg. Chem.,* 2000, **11**, 2401-2408